AEDC-TR-89-4

C#3

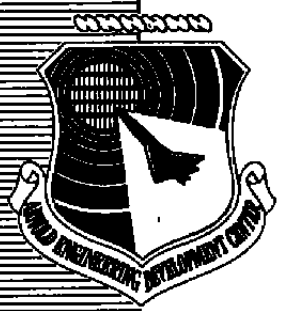

# Wind Tunnel Support System Effects on a Fighter Aircraft Model at Mach Numbers from 0.6 to 2.0

David G. Whitby
Calspan Corporation/AEDC Operations

July 1989

Final Report for Period August 23 – December 1, 1988





**ARNOLD ENGINEERING DEVELOPMENT CENTER**
**ARNOLD AIR FORCE STATION, TENNESSEE**
**AIR FORCE SYSTEMS COMMAND**
**UNITED STATES AIR FORCE**

## NOTICES

When U. S. Government drawings, specifications, or other data are used for any purpose other than a definitely related Government procurement operation, the Government thereby incurs no responsibility nor any obligation whatsoever, and the fact that the Government may have formulated, furnished, or in any way supplied the said drawings, specifications, or other data, is not to be regarded by implication or otherwise, or in any manner licensing the holder or any other person or corporation, or conveying any rights or permission to manufacture, use, or sell any patented invention that may in any way be related thereto.

Qualified users may obtain copies of this report from the Defense Technical Information Center.

References to named commercial products in this report are not to be considered in any sense as an endorsement of the product by the United States Air Force or the Government.

This report has been reviewed by the Office of Public Affairs (PA) and is releasable to the National Technical Information Service (NTIS). At NTIS, it will be available to the general public, including foreign nations.

**APPROVAL STATEMENT**

This report has been reviewed and approved.

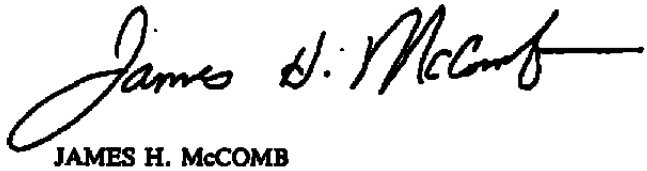

JAMES H. McCOMB
Directorate of Aerospace Flight Dynamics Test
Deputy for Operations

Approved for publication:

FOR THE COMMANDER

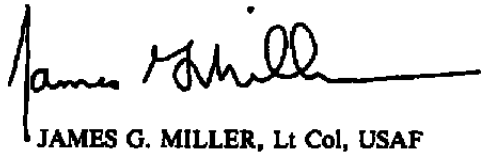

JAMES G. MILLER, Lt Col, USAF
Deputy Director, Directorate of Aerospace Flight
Dynamics Test
Deputy for Operations

UNCLASSIFIED
SECURITY CLASSIFICATION OF THIS PAGE

## REPORT DOCUMENTATION PAGE

Form Approved OMB No. 0704-0188

1a REPORT SECURITY CLASSIFICATION: UNCLASSIFIED

1b RESTRICTIVE MARKINGS:

2a. SECURITY CLASSIFICATION AUTHORITY:

2b. DECLASSIFICATION / DOWNGRADING SCHEDULE:

3. DISTRIBUTION / AVAILABILITY OF REPORT: Approved for public release; distribution is unlimited.

4. PERFORMING ORGANIZATION REPORT NUMBER(S): AEDC-TR-89-4

5. MONITORING ORGANIZATION REPORT NUMBER(S):

6a. NAME OF PERFORMING ORGANIZATION: Arnold Engineering Development Center

6b. OFFICE SYMBOL (If applicable): DO

7a. NAME OF MONITORING ORGANIZATION:

6c. ADDRESS (City, State, and ZIP Code): Air Force Systems Command, Arnold Air Force Base, TN 37389-5000

7b. ADDRESS (City, State, and ZIP Code):

8a. NAME OF FUNDING / SPONSORING ORGANIZATION: Arnold Engineering Development Center

8b. OFFICE SYMBOL (If applicable): DOF

9 PROCUREMENT INSTRUMENT IDENTIFICATION NUMBER:

8c. ADDRESS (City, State, and ZIP Code): Air Force Systems Command, Arnold Air Force Base, TN 37389-5000

10 SOURCE OF FUNDING NUMBERS

| PROGRAM ELEMENT NO. | PROJECT NO | TASK NO | WORK UNIT ACCESSION NO. |
|---|---|---|---|
| 921Z17 | CJ67PG | | |

11. TITLE (Include Security Classification): Wind Tunnel Support System Effects on a Fighter Aircraft Model at Mach Numbers from 0.6 to 2.0

12. PERSONAL AUTHOR(S): Whitby, David G., Calspan Corporation/AEDC Operations

| 13a. TYPE OF REPORT | 13b. TIME COVERED | 14. DATE OF REPORT (Year, Month, Day) | 15 PAGE COUNT |
|---|---|---|---|
| Final | FROM 8/23/88 TO 12/1/88 | July 1989 | 65 |

16. SUPPLEMENTARY NOTATION: Available in Defense Technical Information Center (DTIC).

| 17. COSATI CODES | | |
|---|---|---|
| FIELD | GROUP | SUB-GROUP |
| 14 | 02 | |
| | | |

18 SUBJECT TERMS (Continue on reverse if necessary and identify by block number)

wind tunnel
support interference
sting interference
sting tares
blade interference
blade tares

19 ABSTRACT (Continue on reverse if necessary and identify by block number)

A wind tunnel investigation was conducted using a fighter aircraft model with various sting and blade support system arrangements to evaluate the effects of the model support system on the total body and component longitudinal force and moment data. Total aerodynamic force and moment data were determined from corrected strain-gage balance measured loads. Component data (i.e., tail loads) were obtained by subtracting tail-off balance data from tail-on data. Data taken at free-stream Mach numbers from 0.6 to 2.0 and model angles of attack from -2 to 8 deg were examined. The analysis indicates a significant change in total body and component force coefficients in the presence of various support system configurations. The upper blade tends to decrease drag, lift, and pitching-moment coefficients, while the lower blade generally increases these coefficients. The influence of the sting on aerodynamic coefficients is a function of Mach number and angle of attack. A correction methodology using sting/blade "tares" is proposed and evaluated. The evaluation shows that total body and component force and moment coefficient data are significantly improved using sting/

20. DISTRIBUTION / AVAILABILITY OF ABSTRACT: ☐ UNCLASSIFIED/UNLIMITED ☒ SAME AS RPT. ☐ DTIC USERS

21 ABSTRACT SECURITY CLASSIFICATION: Unclassified

22a NAME OF RESPONSIBLE INDIVIDUAL: Carlton L. Garner

22b TELEPHONE (Include Area Code): (615) 454-7813

22c OFFICE SYMBOL: DOCS

DD Form 1473, JUN 86 — Previous editions are obsolete.

SECURITY CLASSIFICATION OF THIS PAGE
UNCLASSIFIED

19. ABSTRACT. Concluded.
blade "tares" to correct for support system effects.

## PREFACE

The work reported herein was conducted by the Arnold Engineering Development Center (AEDC), Air Force Systems Command (AFSC), under Program Element 921Z17. The results were obtained by Calspan Corporation/AEDC Operations, operating contractor for the Aerospace Flight Dynamics testing effort at the AEDC, AFSC, Arnold Air Force Base, Tennessee. The tests were conducted in the AEDC Propulsion Wind Tunnels (16T and 16S) during the period from March 1 to April 19, 1988 under AEDC Project Numbers CJ67PG and CJ68PG, PWT Test Numbers TF762 and SF211. Data analysis was completed on December 1, 1988, and the manuscript was submitted for publication on June 23, 1989.

## CONTENTS



## ILLUSTRATIONS

## TABLES

# 1.0 INTRODUCTION

Current methods for supporting wind tunnel models invariably require some model geometry changes from the flight vehicle and superimpose the flow field from the support system on the model. These deviations from the flight vehicle environment can induce significant interference into the aerodynamic data. This interference varies considerably with Mach number and the type of support system used. Numerous previous investigations (Refs. 1, 2, and 3, for example) indicate these phenomena for a variety of configurations. Obviously, some method for correcting force and moment data obtained in a wind tunnel must be implemented to obtain interference-free model aerodynamic data for making flight vehicle performance predictions.

The purpose of this analysis is to evaluate support system effects on aerodynamic data. Specifically, the effects of an upper blade, a lower blade, and a sting on fighter aircraft model data are investigated. In addition, this report presents a method for correcting total body and tail load data for support system interference using support system tares, and documents an evaluation of this method for various flight regimes.

Comparisons of support increments, tail loads, and their correction methods are presented for Mach numbers 0.6, 0.8, 0.9, 1.2, 1.5, 1.6, 1.8, and 2.0 and angles of attack of −2, 0, 4, and 8 deg.

The purpose of this report is to reveal conclusions with regard to support system interference using only the applicable data obtained during the tests described above. Therefore, this report does not fully detail the subject tests and presents data only in incremental form.

# 2.0 APPARATUS

## 2.1 TEST FACILITY

The AEDC Propulsion Wind Tunnel (16T) is a variable density, continuous flow tunnel capable of being operated at Mach numbers from 0.06 to 1.6 and stagnation pressures from 120 to 4,000 psfa. The maximum attainable Mach number can vary slightly, depending upon the tunnel pressure ratio requirements with a particular test installation. The maximum stagnation pressure attainable is a function of Mach number and available electrical power. The tunnel stagnation temperature can be varied from about 80° to 160° F, depending upon the cooling water temperature. The tunnel is equipped with a scavenging system which removes combustion products when rocket motors or turbo engines are tested. The test section is 16-ft square by 40 ft long and enclosed by 60-deg inclined-hole perforated walls of 6-percent porosity. The general arrangement of the test section and the test article are shown in Fig. 1.

The AEDC Propulsion Wind Tunnel (16S) is a continuous-flow closed-circuit tunnel presently configured to operate within a Mach number range from 1.6 to approximately 3.4. Operation at Mach numbers between 1.5 and 1.6 and between 3.4 and 4.75 is attainable; however, some tunnel restoration work will be required. Tunnel 16S has a stagnation pressure operating range from about 100 to approximately 2,300 psfa and a current test section stagnation temperature operating range from about 100° to 200°F. The maximum stagnation pressure attainable is a function of Mach number and available electrical power. The maximum stagnation temperature attainable is estimated as approximately 500°F; however, this operating condition will also require some tunnel restoration work. The general arrangement of the test section and the test article location in Tunnel 16S is shown in Fig. 2.

## 2.2 TEST ARTICLE

The test article was a scale model of a fighter aircraft. The model was supported by either a sting or an upper or lower blade arrangement. In addition to the three main support systems, a dummy sting or a dummy blade was attached to the upper blade-supported configuration to evaluate the aerodynamic influence of each support type on the model. Each support system configuration was attached to the facility High-Angle Automated Sting (HAAS) support system in Tunnel 16T and the High Pitch Sting Support System in Tunnel 16S. A representation of the model with the lower blade support configuration is shown installed in Tunnel 16T in Fig. 1 and in Tunnel 16S in Fig. 2. Each of the model support arrangements is shown in Fig. 3, and sting and blade support hardware details are shown in Fig. 4.

Model aerodynamic data were corrected for flow-through duct drag and for model base and cavity pressure tares. The sting shroud was a metric model component (i.e., the balance sensed the loads associated with the shroud), and it is shown surrounding both the sting and dummy sting in Fig. 3.

## 2.3 INSTRUMENTATION

A six-component strain-gage balance was used to measure aerodynamic forces on the model. The balance outputs were recorded on the Tunnel 16T and Tunnel 16S data acquisition systems and transmitted to the facility computer for calculation of corrected force and moment coefficients.

The model surface, cavity, internal flow duct, and base pressures were measured by three 15-psid, 48-port ESP modules.

The model pitch angle was determined from standard HAAS and high pitch system instrumentation and verified by a Schaevitz angular position indicator located in the model. Thermocouples were used to monitor the temperature of the balance and the ESP transducers.

# 3.0 TEST DESCRIPTION

## 3.1 TEST CONDITIONS AND PROCEDURES

For this study, data were obtained at free-stream Mach numbers of 0.6, 0.8, 0.9, 1.2, 1.5, 1.6, 1.8, and 2.0 at a constant unit Reynolds number of 2.0 x $10^6$/ft in Tunnel 16T and 1.5 x $10^6$/ft in Tunnel 16S.

Data were obtained by establishing the appropriate test section flow conditions and model attitude (model angles of attack used in this report are −2, 0, 4, and 8 deg) and recording steady-state data. The variation of model angle of attack and data acquisition were computer controlled.

All steady-state measurements were sequentially recorded by the facility on-line computer system, which reduced the data to engineering units, further processed the data to obtain the required model parameters, tabulated the data in the tunnel control rooms, recorded the data on digital magnetic tape, and transmitted the data to the AEDC central computer file. The data stored in the central computer file were generally available for plotting and analysis with the PWT Interactive Graphics System within 30 sec after aquisition. The immediate availability of the tabulated and plotted data permitted continual on-line monitoring of the test results.

## 3.2 CORRECTIONS

The balance-measured forces and moments were corrected for sensed changes in model weight, model base and cavity pressure forces, and internal duct flow forces. Upper and lower blade cavity pressures were used to correct normal-force and pitching-moment coefficients. Upper blade cavity pressures were also used to correct axial force since some slope existed on the upper surface of the model.

The sting support configuration used a metric shroud to fair the portion of the model smoothly where the sting entered. Balance data were corrected for shroud base and cavity drag but not for normal force or pitching moment resulting from this shroud. Since it was a metric component but did not represent true geometry, the shroud is thought to have introduced some error which was not corrected for in normal force and pitching moment. Model pitch angle was corrected for flow angularity in both wind tunnels.

## 3.3 DATA REDUCTION

The facility standard force and moment data reduction program was used to compute model aerodynamic loads from balance outputs. The corrected balance forces were converted to body and stability axes coefficients based on model wing reference area (S), wing span (b), and mean aerodynamic chord ($\bar{c}$).

Exit plane rake pressures were used to calculate internal duct drag for the flow-through ducts. Model pressures were reduced to coefficient form based on free-stream conditions. Pressure substitution and bad-coding were provided when measured pressures were not available or deemed incorrect. The total aerodynamic loads on the model were obtained by summing the balance measured loads and the appropriate tare loads and corrections.

Model attitude was calculated from measured sting support pitch and roll angles with corrections for balance/sting angular deflection and wind tunnel flow angularity.

### 3.4 UNCERTAINTY OF MEASUREMENTS

Uncertainties (combinations of systematic and random errors) of the basic tunnel parameters, shown in Fig. 5, were estimated from repeat calibrations of the instrumentation and from the repeatability and uniformity of the test section flow during tunnel calibration. Uncertainties in the instrumentation systems were estimated from repeat calibrations of the systems against secondary standards whose uncertainties are traceable to the National Institute of Standards and Technology (NIST) calibration equipment. The tunnel parameter and instrument uncertainties, for a 95-percent confidence level, are combined using the Taylor series method of error propagation described in Ref. 4 to determine the uncertainties of the reduced parameters shown in Table 1 for selected test conditions.

Repeatability of data used for this investigation is shown in Table 2. Both maximum repeatability values and average repeat data based on the number of repeat runs for a given condition are presented. Generally the repeatability values are somewhat less than the data uncertainty at the corresponding test condition. Occasionally, however, the repeatability is more on the order of twice the uncertainty. Repeat comparisons using data obtained at the very start of testing in each wind tunnel are included, and it is assumed that installation effects and balance zero shifts are the major contributors when such large repeat data discrepancies occur.

## 4.0 RESULTS AND DISCUSSION

### 4.1 DATA PRESENTATION

For this analysis, data were obtained with the five support system configurations shown in Fig. 3. Drag, lift, and pitching-moment coefficients for the configurations were then subtracted as illustrated in Fig. 6 to obtain support increments. Figure 6 shows how support increments were obtained for both tail-on and tail-off configurations for each of the three main support configurations.

The computer program used to obtain data increments fits drag, lift, and pitching-moment coefficients as functions of angle of attack using a least-squares, third-order polynomial curve fit. The program then calculates increments at specific angles of attack from the curve fits. The increments are plotted in Figs. 7 – 8. The same method was used to obtain repeatability values at discrete angles of attack (see Table 2).

Data for the five configurations in Fig. 3 were also obtained at discrete angles of attack from the curve fits. These data, along with the support increments described above, were then combined as shown in Fig. 9, resulting in corrected data. These five support corrections are evaluated by presenting them relative to a baseline or reference correction. For comparing support increments in this study, data derived from Case 1 (see Fig. 9) are defined as the baseline. Case 1 reference data were subtracted from data for each of the other cases. The five sets of corrected data are presented relative to the baseline data in Fig. 10.

Tail loads were obtained using an incremental method shown in Fig. 11. Two tail increment corrections ("lower blade corrected" and "sting corrected") were employed by combining data from various configurations as shown in Fig. 12. The data plotted in Fig. 13 represent both the corrected and uncorrected (influenced by the support system) tail loads. Similar to the presentation of total body loads, tail loads are plotted referenced to a set of baseline data. For Fig. 13, the baseline data are the "lower blade corrected" data.

## 4.2 TOTAL BODY LOADS

### 4.2.1 Support System Increments

The contribution of the support configuration to the total body lift, drag, and pitching-moment coefficients is shown in Figs. 7 – 8. Force and moment coefficients are plotted versus Mach number for both the tail-on configurations (Fig. 7) and tail-off configurations (Fig. 8). Each figure consists of drag, lift, and pitching-moment coefficient plots. The Mach number scale on the abscissa is split at M = 1.6, which is repeated. Data at Mach number 1.6 were obtained in both wind tunnels (16T and 16S), and each data set is presented.

A comparison of the drag coefficient data from the two blade configurations indicates that the lower blade generally has the larger effect which is to produce a higher drag coefficient. The upper blade often has the effect of decreasing drag coefficient, especially subsonically. At low angles of attack (alpha = −2 and 0 deg), the difference between the effects of upper and lower blade on drag coefficient is moderate (less than 0.0020) subsonically and low (less than 0.0010) supersonically. As model angle of attack is increased to 4 and 8 deg, the difference between upper and lower blade effects increases considerably at Mach numbers between 0.9

and 1.2. Alhough the magnitude of the blade effects is a function of angle of attack, the directions of the effects generally remain consistent as angle of attack changes.

The sting's effect on total body drag coefficient is a strong function of both Mach number and angle of attack. At low angles of attack, the sting decreases drag coefficient even more than the upper blade, while at higher angles, it increases drag coefficient more than the lower blade. The sting and shroud effectively pressurize the lower surface through which they enter the model, yielding a decrease in drag coefficient at negative angles of attack and an increase in drag coefficient at positive angles. The effects are the same in direction across the Mach number range, but they are significantly larger at supersonic Mach numbers.

Upper and lower blades produce nearly equal decreases and increases in lift coefficient, respectively. Subsonically, the blade lift coefficient increments are nearly symmetric about the x-axis. The blades act as spoilers, pressurizing the surfaces through which they enter the model. The differences between upper and lower blade increments are small at Mach number 0.6 , but at Mach numbers above 0.6, the differences increase significantly.

The sting lift coefficient increments are high positive values relative to those of the lower blade for all Mach numbers and angles of attack. Lift coefficient was not corrected for the metric shroud surrounding the sting; therefore, these results are explained by the sting shroud acting as a flap deflected positively to increase lift.

It is interesting to note that lift coefficient increment signs and magnitudes for each support configuration are nearly independent of angle of attack. This observation is in contrast to the large angle-of-attack effects measured for drag coefficient.

Upper and lower blades also produce nearly equal decreases and increases in pitching-moment coefficient, respectively. The pitching-moment coefficient increments for Mach numbers up to 1.6 are practically symmetric about the x-axis. The differences between upper and lower blade increments are nearly constant at subsonic Mach numbers and decrease steadily as supersonic Mach number increases.

The increase/decrease in pitching-moment coefficient with a corresponding increase/decrease in lift coefficient indicates that the major influence of the strut is to pressurize the model surface in front of the model's center of pressure.

The sting produces a very small pitching-moment coefficient increment subsonically and a distinctly negative increment supersonically. Therefore, it is concluded that at subsonic Mach numbers, the interference region of the sting is essentially centered about the model center of pressure. Even though the model center of pressure shifts aft at supersonic Mach

numbers, the interference region of the sting at these Mach numbers is centered even farther aft, causing a negative increment in pitching moment coefficient.

As with the lift coefficient, pitching-moment coefficient increments for each support system arrangement are practically independent of model angle of attack.

When the data in Fig. 7 are compared with the corresponding data in Fig. 8 , the tail seems to have no effect on the sign of support effects. The magnitude of the support increments is very similar but generally smaller in the absence of the tail. This observation leads to the conclusion that the support increments described above tend to be independent of small changes in configuration.

The tendency for the direction of sting and blade increments to be configuration independent is reinforced by the data contained in Refs. 2 and 3. Lower blade and/or sting arrangements, similar to that used during this investigation, were used for two cargo/transport configurations at subsonic Mach numbers. The effects of the support systems on drag and pitching-moment coefficients reported in Refs. 2 and 3 are consistent with the corresponding effects in this study.

Even though the effect of the support system on the sign of longitudinal force and moment coefficients is consistent between the three configurations, the magnitude of support increments varies between configurations. Figures 7 – 8 show a large influence of support system on aerodynamic coefficients (relative to the uncertainty) which must be removed from the data to achieve accurate information.

### 4.2.2 Correction Methodology

To account for the appreciable effects of the support system described above, a set of corrections using sting/blade "tares" is proposed and evaluated. Figure 9 shows the five cases which were applied to the data in this report. Logically, a sixth case using the upper blade tail-on configuration would follow, but this method would be identical to Case 1.

Each of the cases in Fig. 9 was applied to the uncorrected data base to obtain total body loads with support system interference tares removed. The support system tare correction methodology is evaluated by checking how well and for which conditions the five cases agree.

As described in Section 4.1 of this report, the baseline (Case 1) data were subtracted from data for each of the other cases. For this reason, the abscissa is actually one of the five cases for the purposes of Fig. 10. The "Figure of Merit" used to evaluate correction method agreement is plus or minus the uncertainty (effectively twice the uncertainty). The uncertainty

bands shown in Fig. 10 are only those associated with absolute aerodynamic coefficient data and not incremental data. Without knowledge of the magnitude of aerodynamic coefficients deemed significant to impact aircraft performance, this uncertainty band represents only a "Figure of Merit" to evaluate the correction methodology. For the purposes of this report, the uncertainty band is an arbitrary basis for comparison of corrections. Since the baseline correction was chosen arbitrarily and is not necessarily the correct answer, the uncertainty band is moved to surround as much of the data as possible.

A comparison of Fig. 10 with Figs. 7 – 8 reveals that differences between sets of corrected drag coefficient data are significantly less than the corresponding support interference increments. For example, the average absolute support increment in drag coefficient at alpha = 8 deg with the tail on is 0.0026 (see Fig. 7d), but the average deviation of the corrected data from baseline data is 0.0012 for the same conditions (see Fig. 10d). In fact, at low angles of attack (alpha = −2, 0, and 4 deg), the five cases agree to within the uncertainty band described above. At 8-deg angle of attack, only the subsonic Mach number data agree well enough to conclude that the cases converge to the correct drag coefficient.

Although some lift coefficient data fall outside the uncertainty band for Mach numbers between 0.9 and 1.6, the corrected data agree better than the magnitude of the original support increments. Using alpha = 8 deg with the tail on as an example, the average absolute support increment in lift coefficient is 0.0117 (see Fig. 7d), while the average deviation of corrected data from the baseline data is 0.0051 (see Fig. 10d).

For pitching-moment coefficient, the five cases agree better than the magnitude of the support increments again, but nowhere does the correction method collapse all data to within the uncertainty band described above. Especially at Mach number 1.2, the support increments do not collapse to within data uncertainty, but a considerable improvement of the data is still observed. For example, at alpha = 8 deg with the tail on, the average absolute support increment in pitching-moment coefficient across the Mach number range is 0.0084 (see Fig. 7d), while the average deviation of corrected data from the baseline data is 0.0034 for the same conditions (see Fig. 10d).

## 4.3 TAIL LOADS

### 4.3.1 Support System Effects

The effect of the upper blade, lower blade, and sting support configurations on tail loads was investigated by subtracting test data as shown in Fig. 11. The data represented by the open symbols in Fig. 13 are referenced to a baseline (see Section 4.1). The closed symbols in Fig. 13 represent corrected tail load data which will be discussed in Section 4.3.2. Effects

of support system on tail drag coefficient exist, but they are on the order of the data uncertainty. Tail lift coefficient increments attributable to the support system are slightly greater than data uncertainty, especially at Mach number 1.2. Tail pitching-moment coefficient increments fall outside the data uncertainty band at all Mach numbers with the largest effect at Mach number 1.2. The effects increase slightly as angle of attack increases.

### 4.3.2 Correction Methodology

Two cases shown in Fig. 12, "lower blade corrected" and "sting corrected," were used to obtain corrected tail load data. The corrected tail loads based on the two cases are shown along with the tail loads in the presence of the support system in Fig 13. The format and scales for these figures are identical to those of Figs. 7, 8, and 10. The "lower blade corrected" case was used as a baseline and is therefore represented by the abscissa. The evaluation of the support tares method of correction is again based upon the agreement of the two corrections in Fig. 12. In Fig. 13, the abscissa and the closed circles represent these two corrections, so the degree to which the closed circles follow the x-axis is a measure of the consistency of the correction method.

Even though the data in the presence of the support system are often inside the uncertainty bands themselves, the corrected data agree significantly better than the uncorrected tail support increments. The closed circles in Fig. 13 nearly always fall to within the arbitrary uncertainty band of the abscissa (pitching moment is the best example).

## 5.0 CONCLUSIONS AND RECOMMENDATIONS

An analysis was conducted to evaluate support system interference using a fighter aircraft model. Various support system configurations were used with appropriate dummy sting and blade models to assess the influence of an upper blade, a lower blade, and a sting on the longitudinal aerodynamic coefficients and tail loads of an aircraft model. Appreciable support system effects are found to exist for both total body and tail loads. In general, the upper blade decreases drag, lift, and pitching-moment coefficients, and the lower blade increases the coefficients. The sting's effect on forces and moments varies significantly with Mach number and angle of attack.

A correction methodology using support "tares" is presented and evaluated. Several combinations of support tares were applied to the wind tunnel data. The corrections are evaluated by examining how well and for which conditions they agree. The basis used for this comparison is the absolute aerodynamic coefficient uncertainty, which is only an arbitrary "Figure of Merit." This analysis shows that drag coefficient can be significantly improved using sting/blade tares except at supersonic Mach numbers at high angles of attack. This

result suggests that minimum drag data could be one application for the use of support tares to correct for support system effects. Although lift coefficient corrections do not collapse to within the data uncertainty for all Mach numbers and pitching-moment coefficient corrections rarely collapse based on data uncertainty and repeatability, lift and pitching moment data are improved by applying support tares. Failure of the correction methodology to collapse all the data is attributed to several factors. The first of the factors are the basic limitations embedded in the sting/blade tares methodology which would include secondary effects such as mutual interference between the actual and dummy support systems. Also contributing to lack of agreement are installation effects from installation and removal of the various configurations and temperature effects resulting in balance shifts which could not be controlled.

A similar correction methodology was applied to tail force and moment coefficients. In this case, drag, lift, and pitching-moment coefficient corrections were found to collapse to within the data uncertainty described above.

## REFERENCES

1. Alstatt, M. C. and Dietz, W. E. "Support Interference on an Ogive-Cylinder Model at High Angle of Attack in Transonic Flow." AEDC-TR-78-8 (AD-A051689), March 1978.

2. Carter, E. C. "Interference Effects of Model Support Systems." AGARD-R-601, April 1975, pp. 3.1 - 3.10.

3. Wells, O. D., et al. "Preliminary Analysis of the C-17A Phase II Configuration Development Model Test in the Rockwell International 7-Foot Trisonic Wind Tunnel." Douglas Aircraft Company Report MDC J9517.

4. Abernethy, R. B. and Thompson, J. W., Jr. "Handbook—Uncertainty in Gas Turbine Measurements." AEDC-TR-73-5 (AD755356), February 1973.

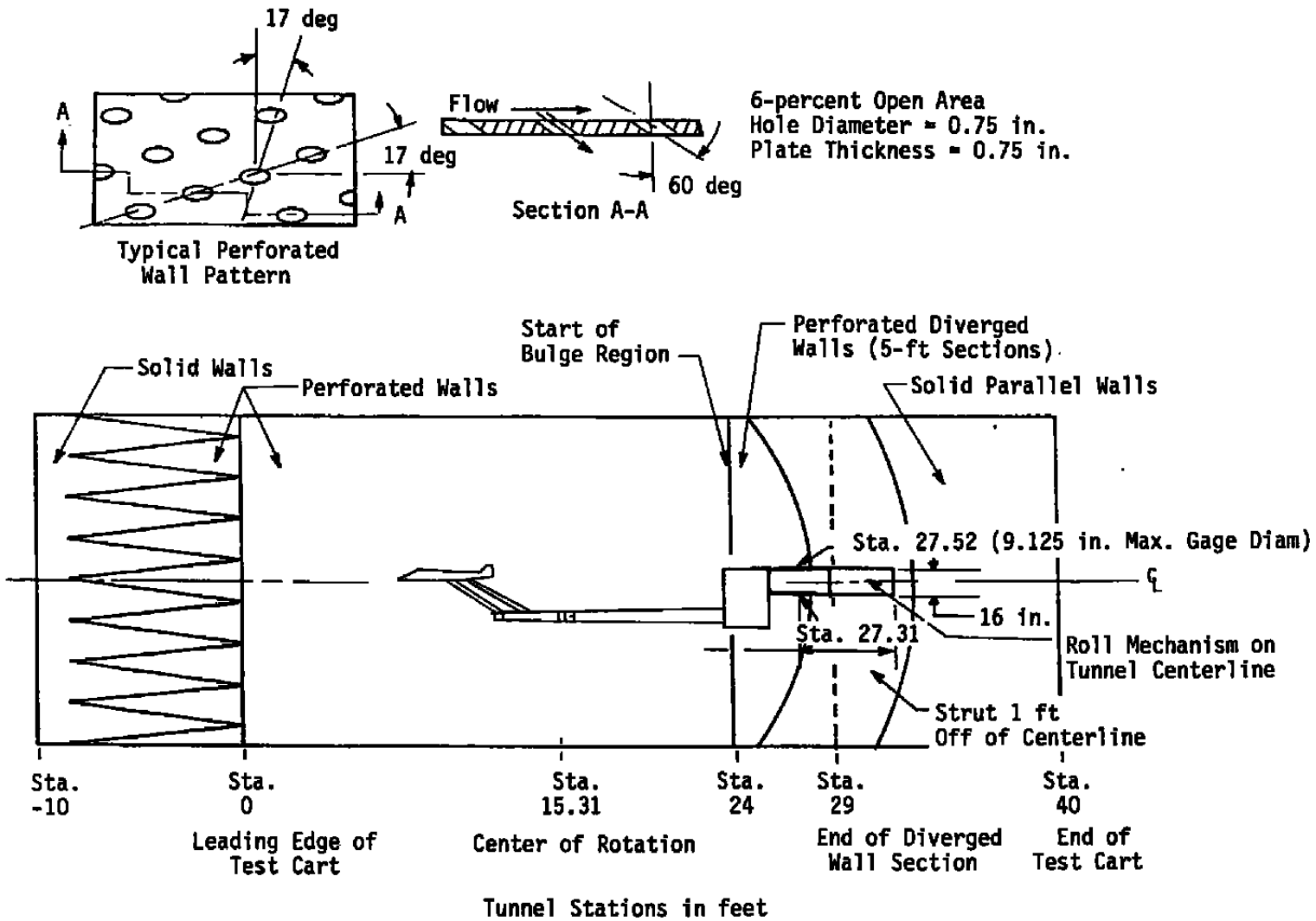


**Figure 1. Model installation in Propulsion Wind Tunnel (16T).**

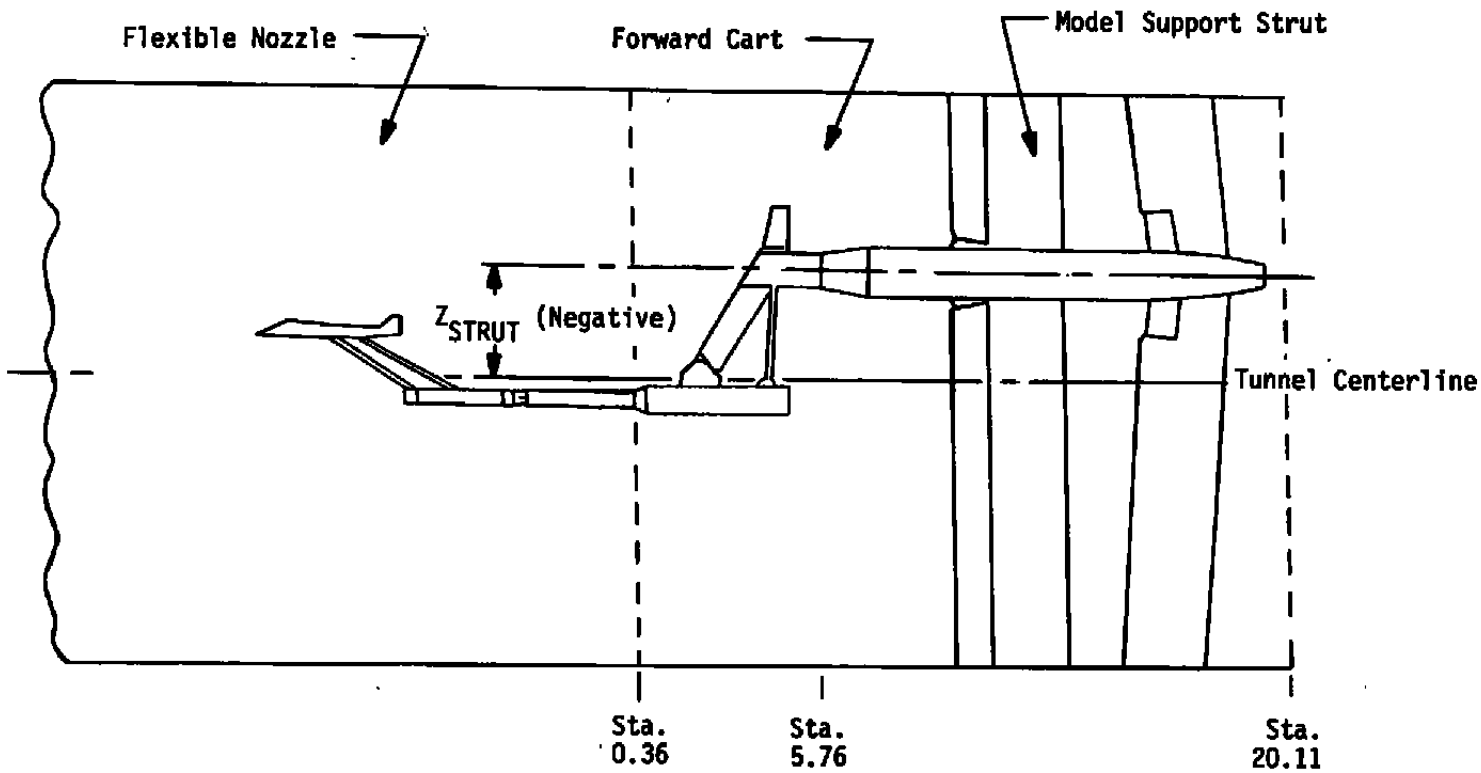


**Figure 2. Model installation in Propulsion Wind Tunnel (16S).**

Lower Blade

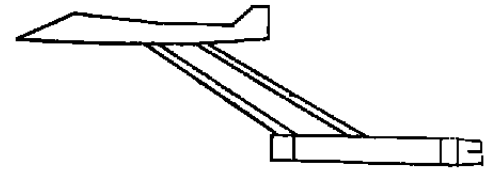

Sting

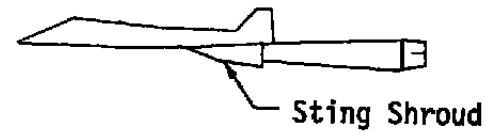


Upper Blade

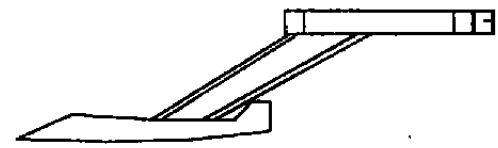

Upper Blade, Dummy Sting

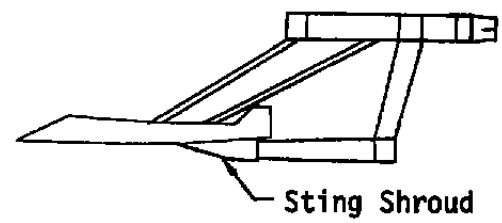


Upper Blade, Dummy Lower Blade

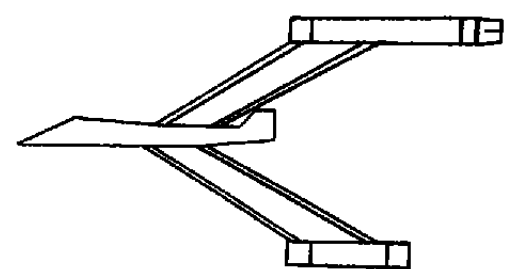

**Figure 3. Support configurations.**

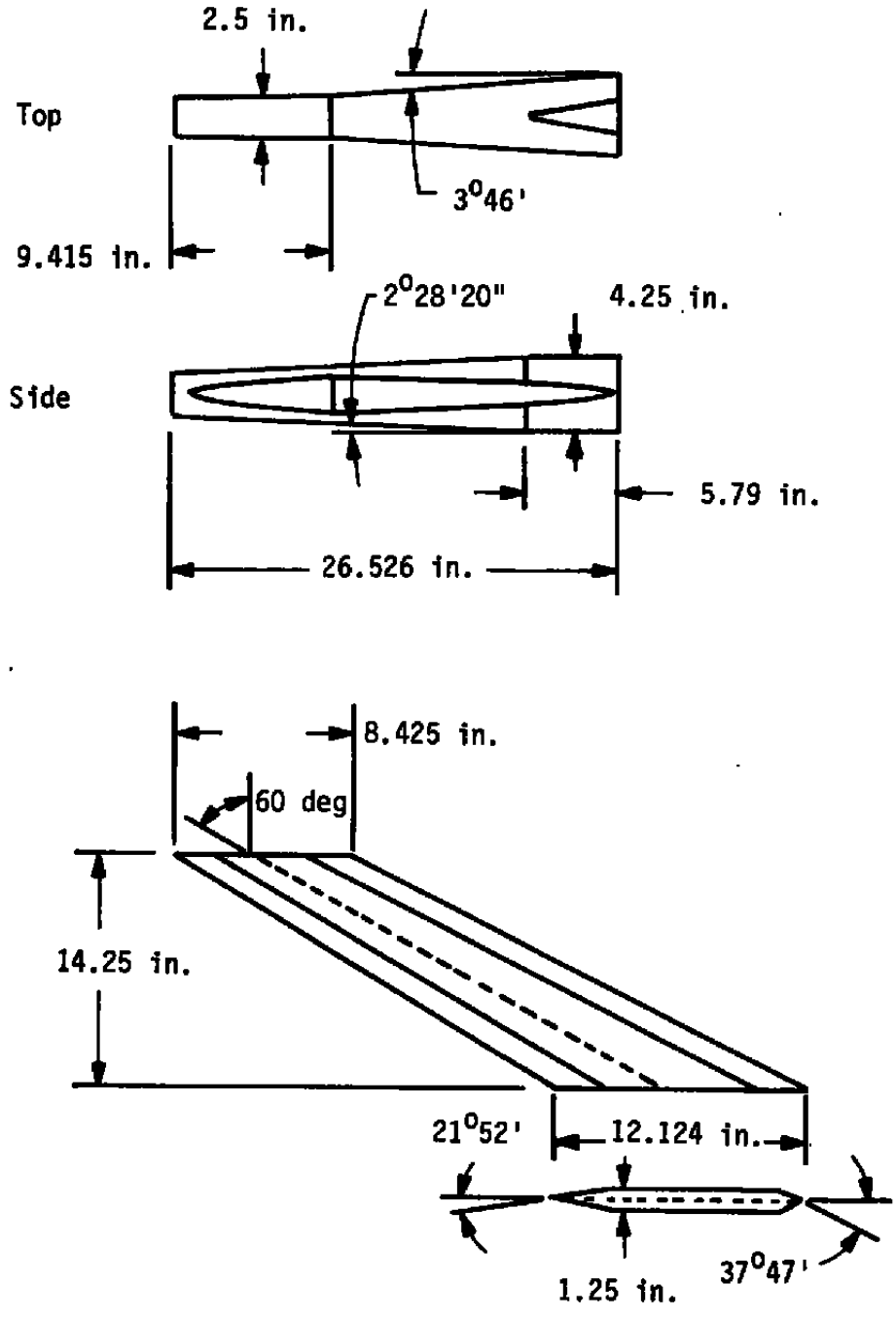


Note: Upper blade indentical to lower blade

**Figure 4. Sting and blade support hardware details.**

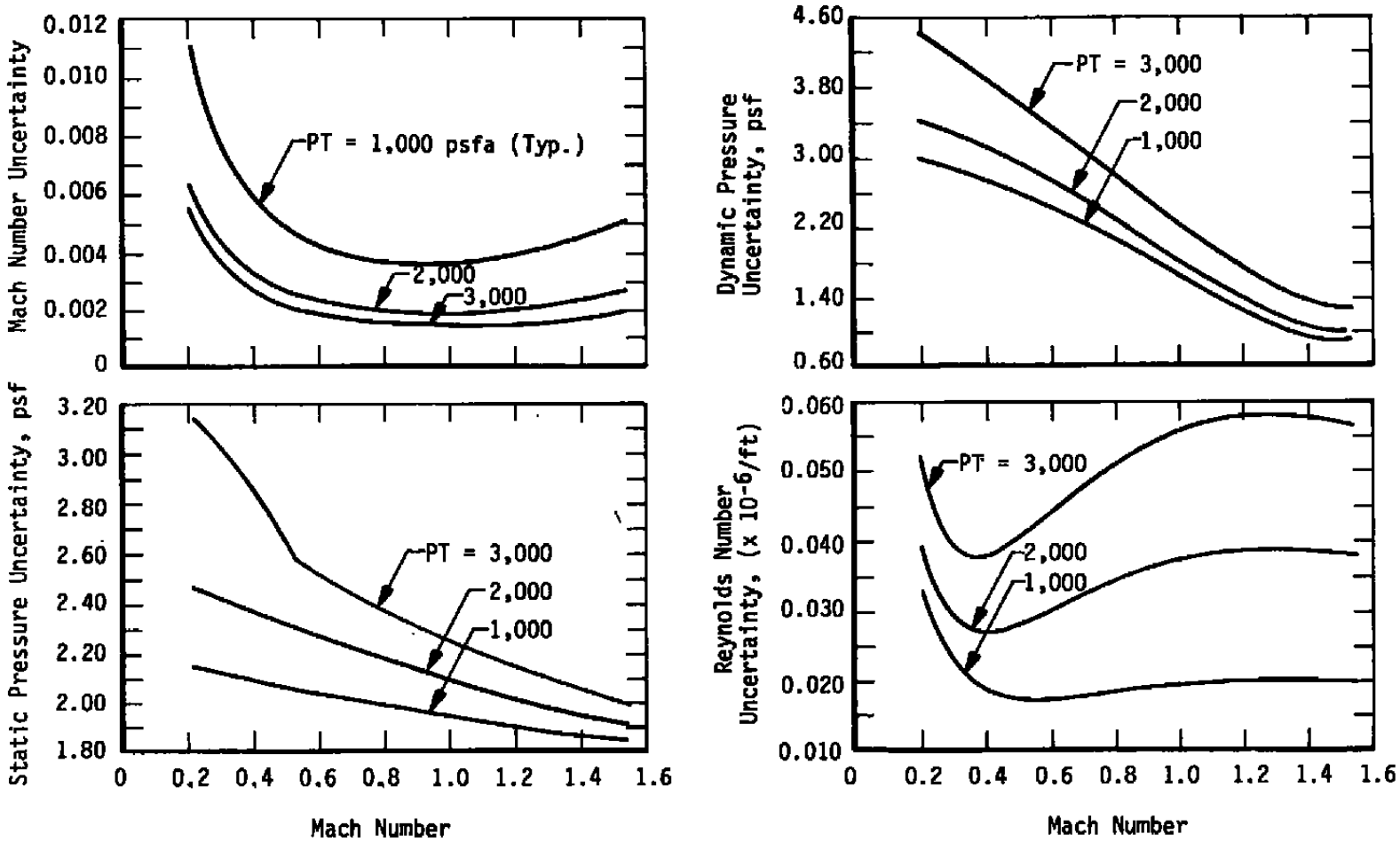


**Figure 5. Uncertainties of basic wind tunnel parameters.**

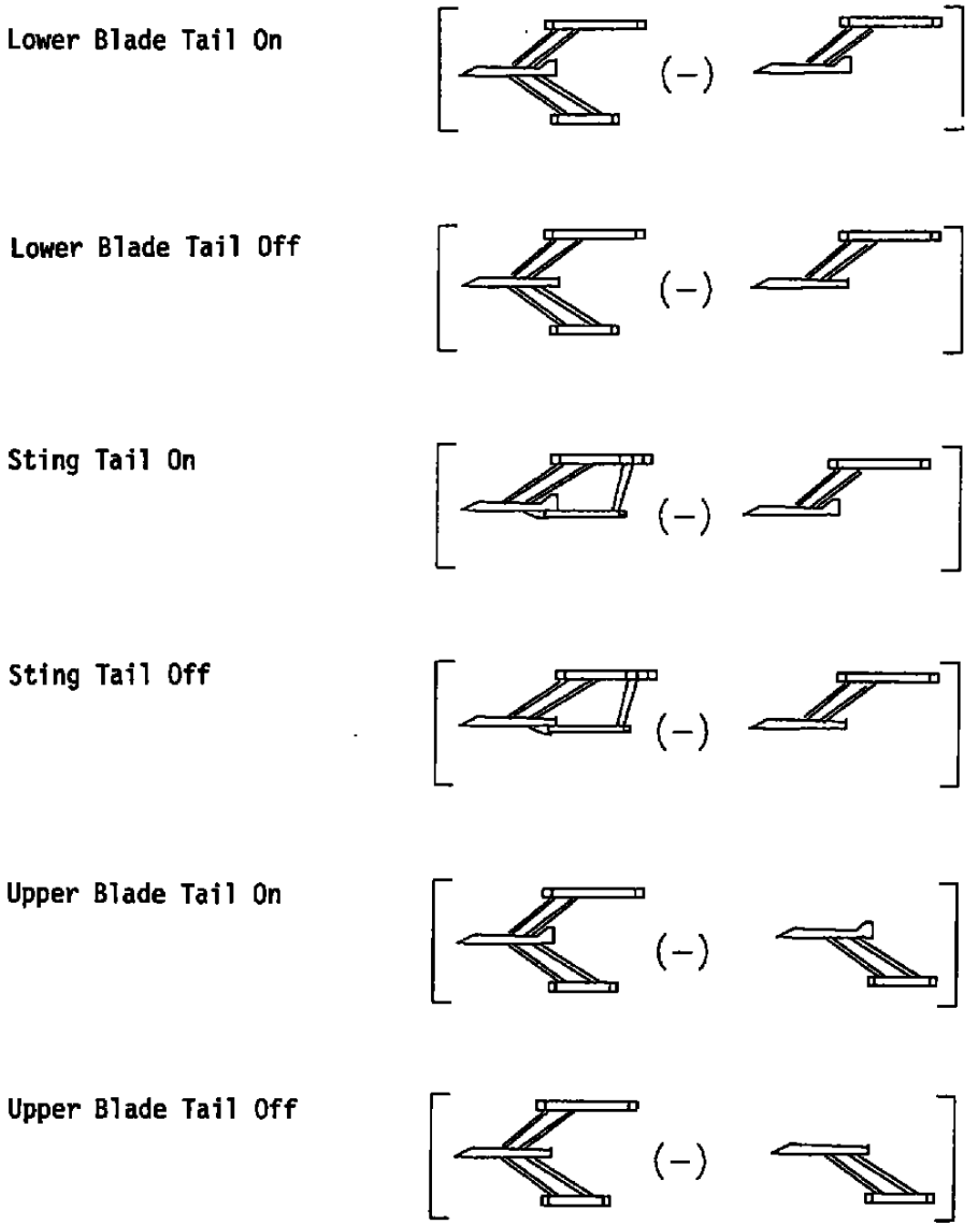


**Figure 6. Support increments.**

■ Lower Blade Tail On

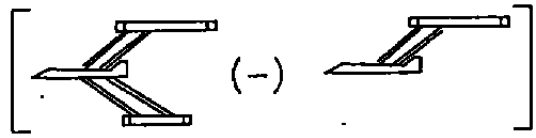

● Sting Tail On

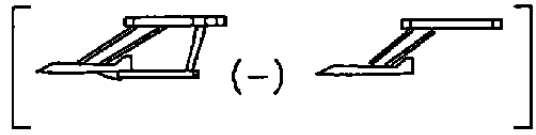

◆ Upper Blade Tail On

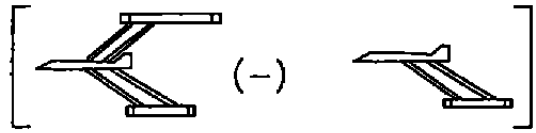

**Legend for Figure 7a**

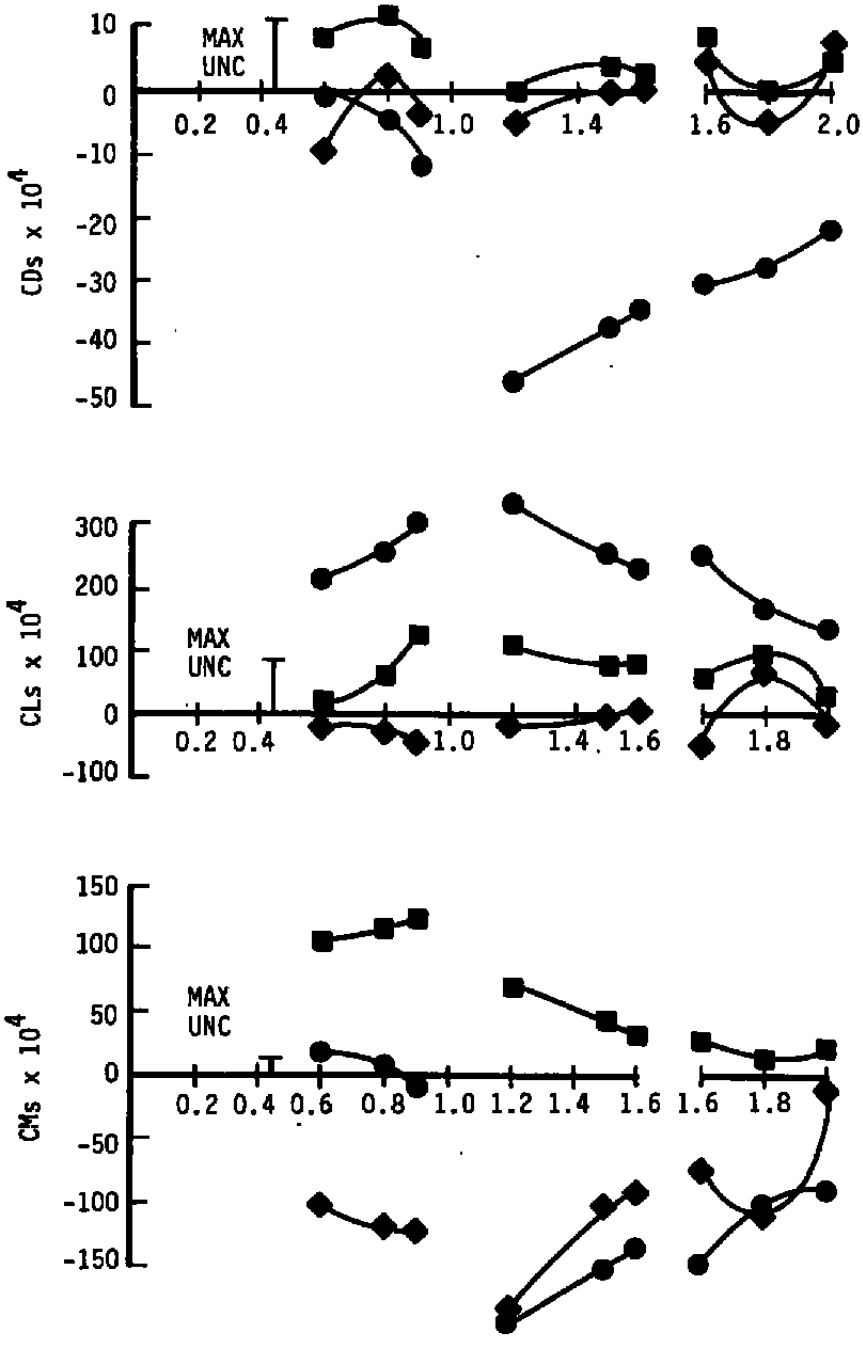


**a. Alpha = −2 deg**

**Figure 7. Comparison of support effects, tail on.**

■ Lower Blade Tail On

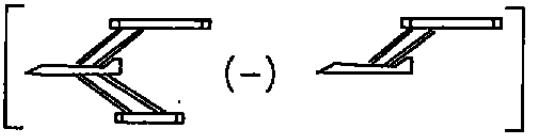


● Sting Tail On

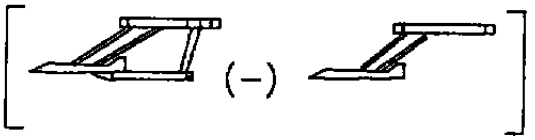


◆ Upper Blade Tail On

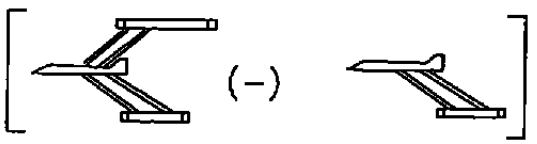


**Legend for Figure 7b**

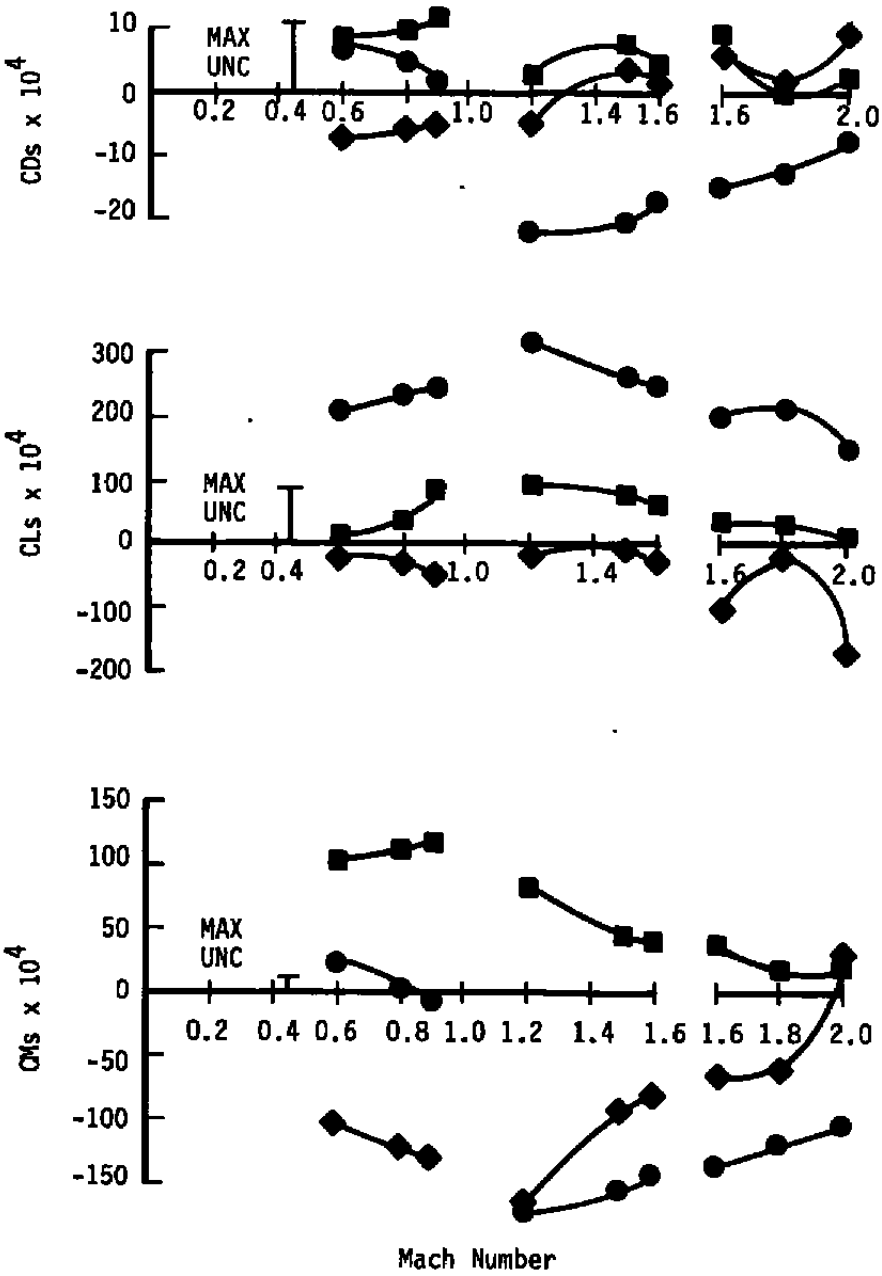


**b. Alpha = 0 deg**

**Figure 7. Continued.**

■ Lower Blade Tail On

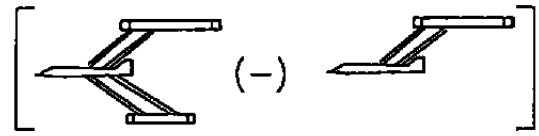


● Sting Tail On

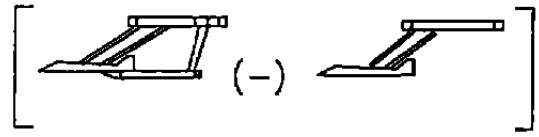


◆ Upper Blade Tail On

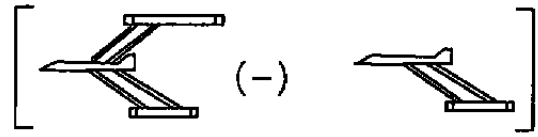


**Legend for Figure 7c**

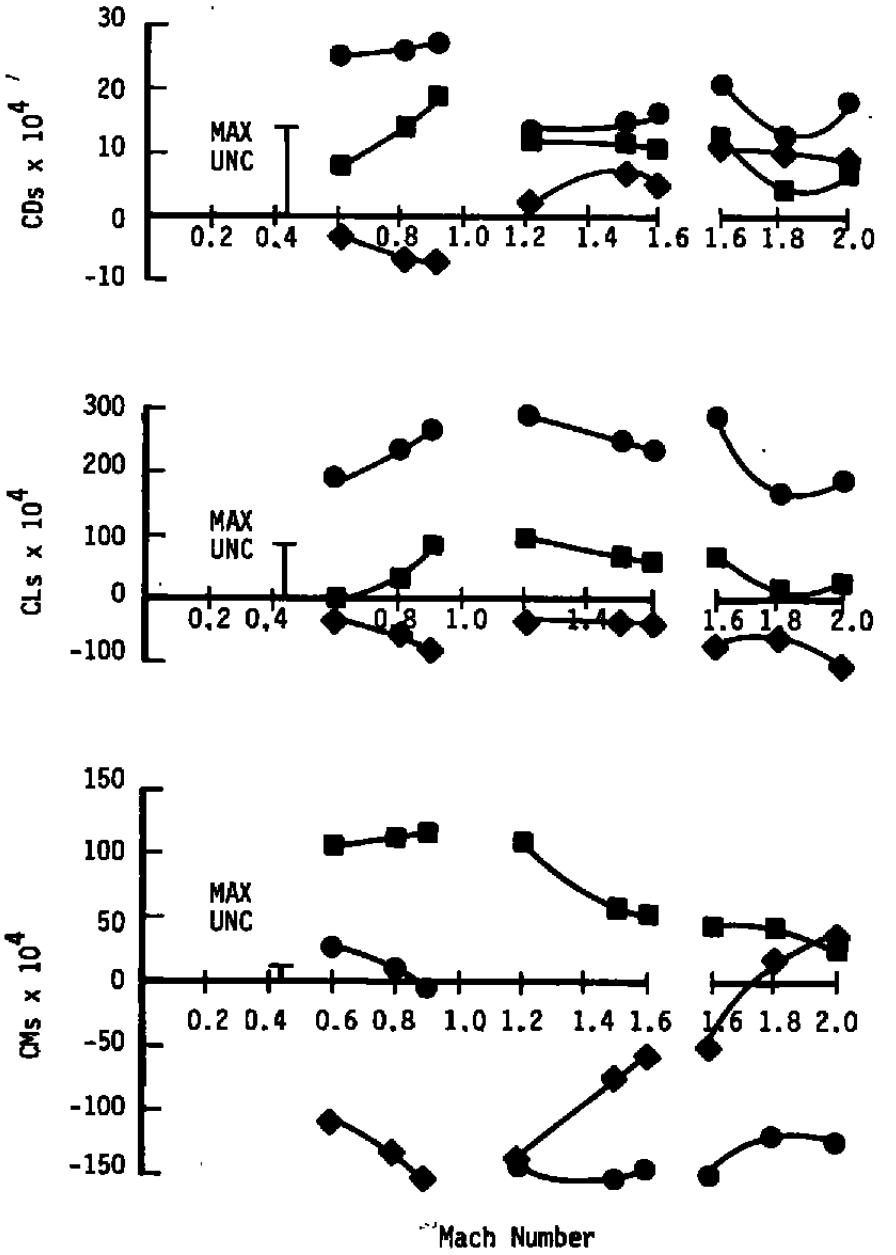


c. Alpha = 4 deg

**Figure 7. Continued.**

■ Lower Blade Tail On

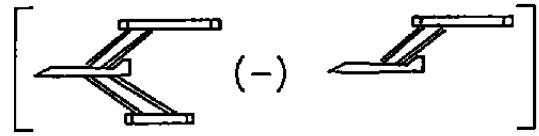


● Sting Tail On

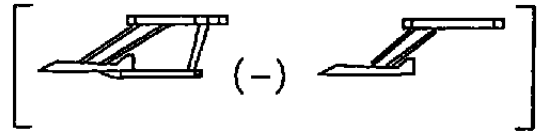


◆ Upper Blade Tail On

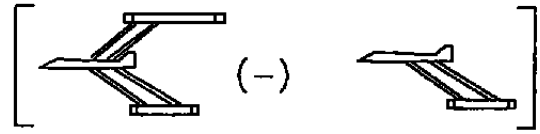


**Legend for Figure 7d**

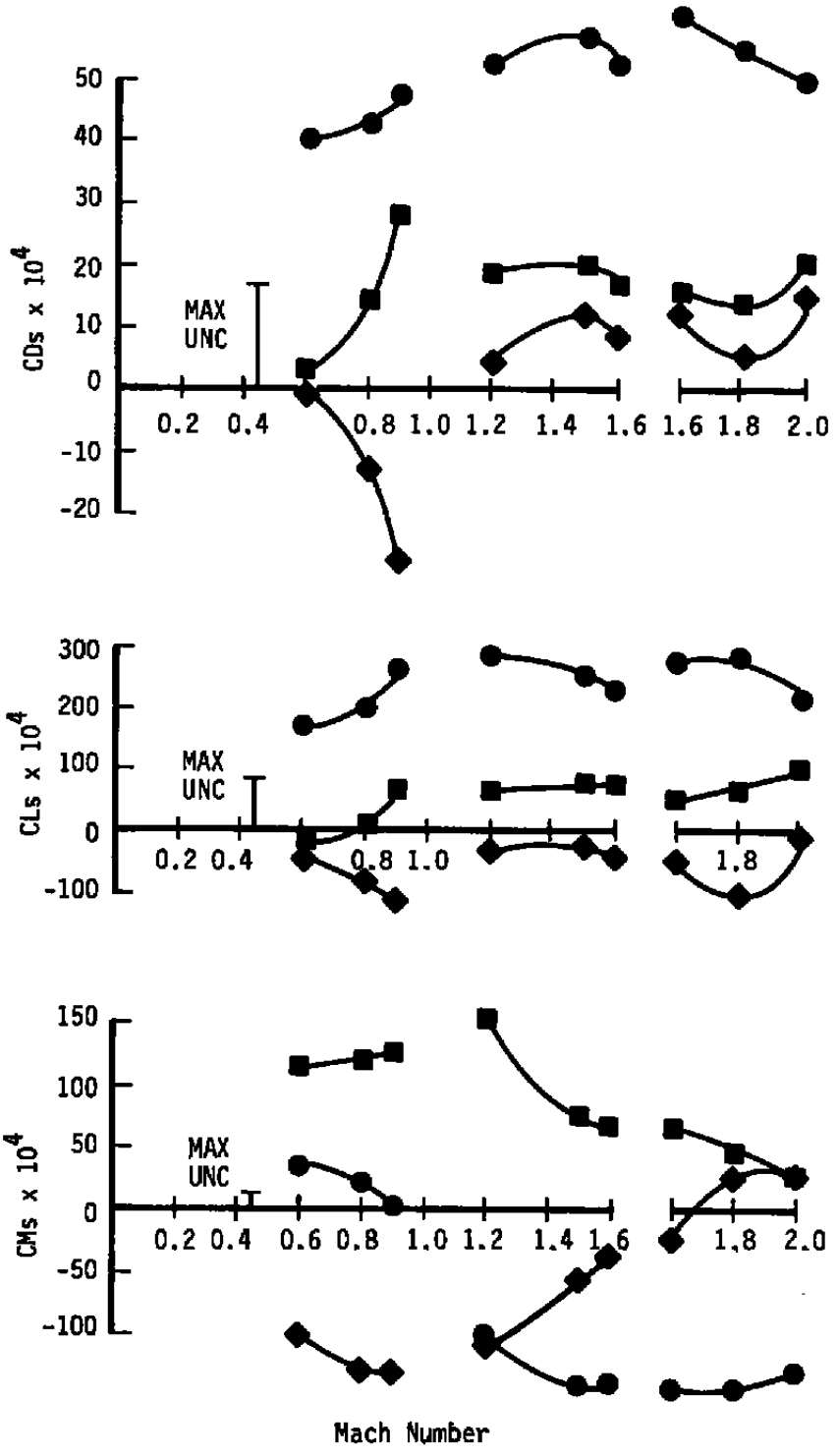


**d. Alpha = 8 deg**

**Figure 7. Concluded.**

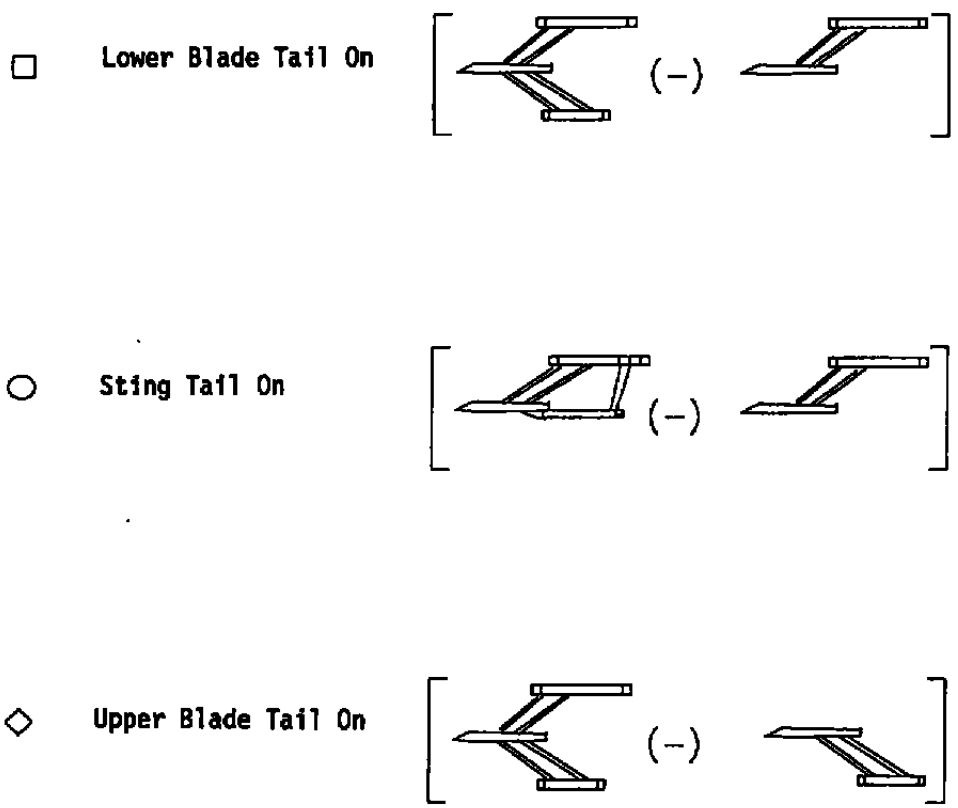


**Legend for Figure 8a**

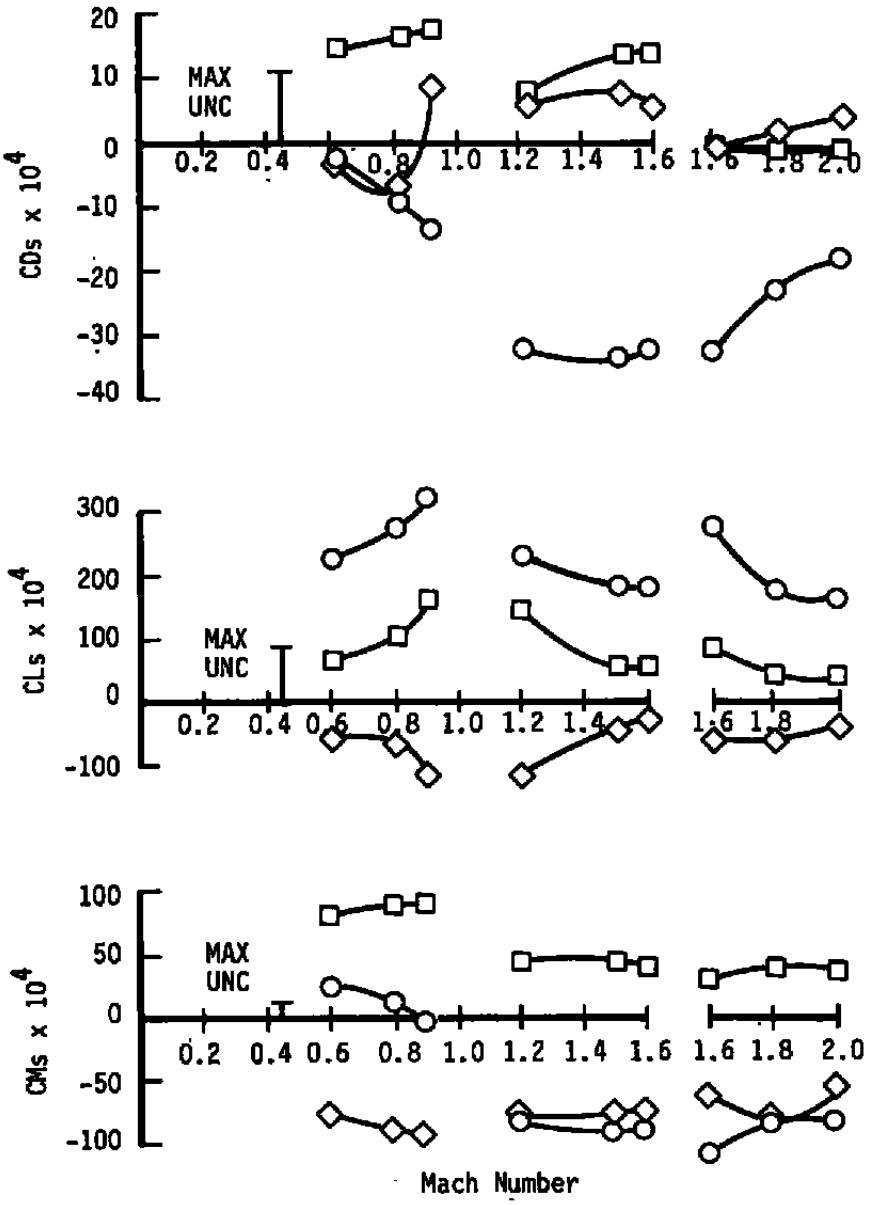


a. Alpha = −2 deg

**Figure 8. Comparison of support effects, tail off.**

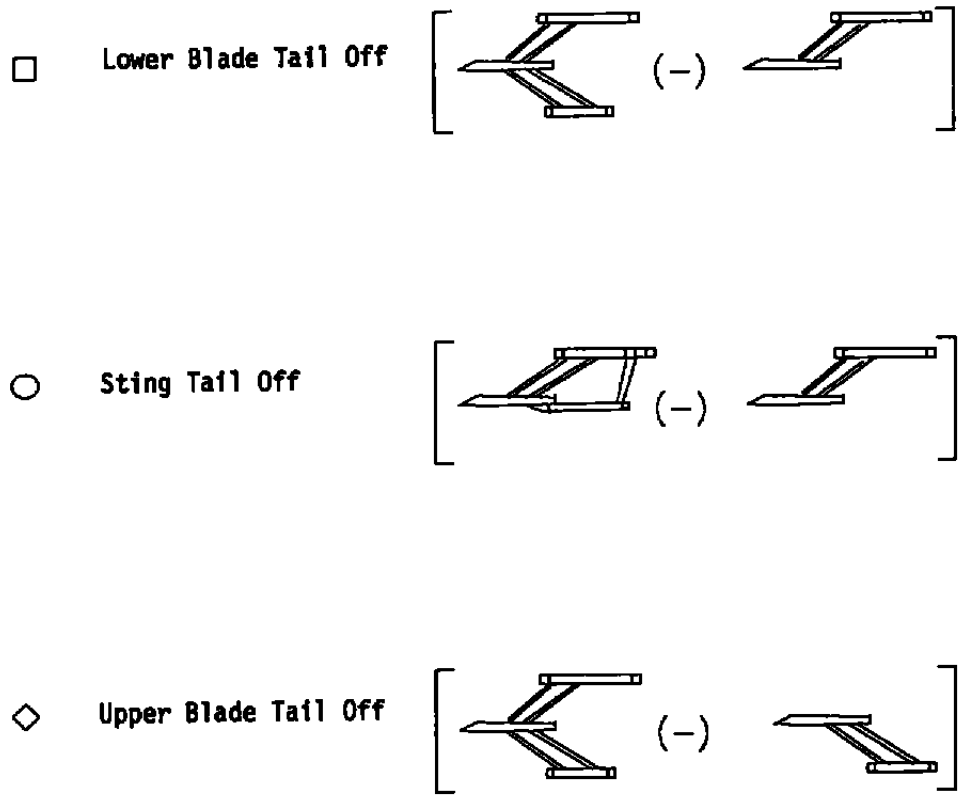


**Legend for Figure 8b**

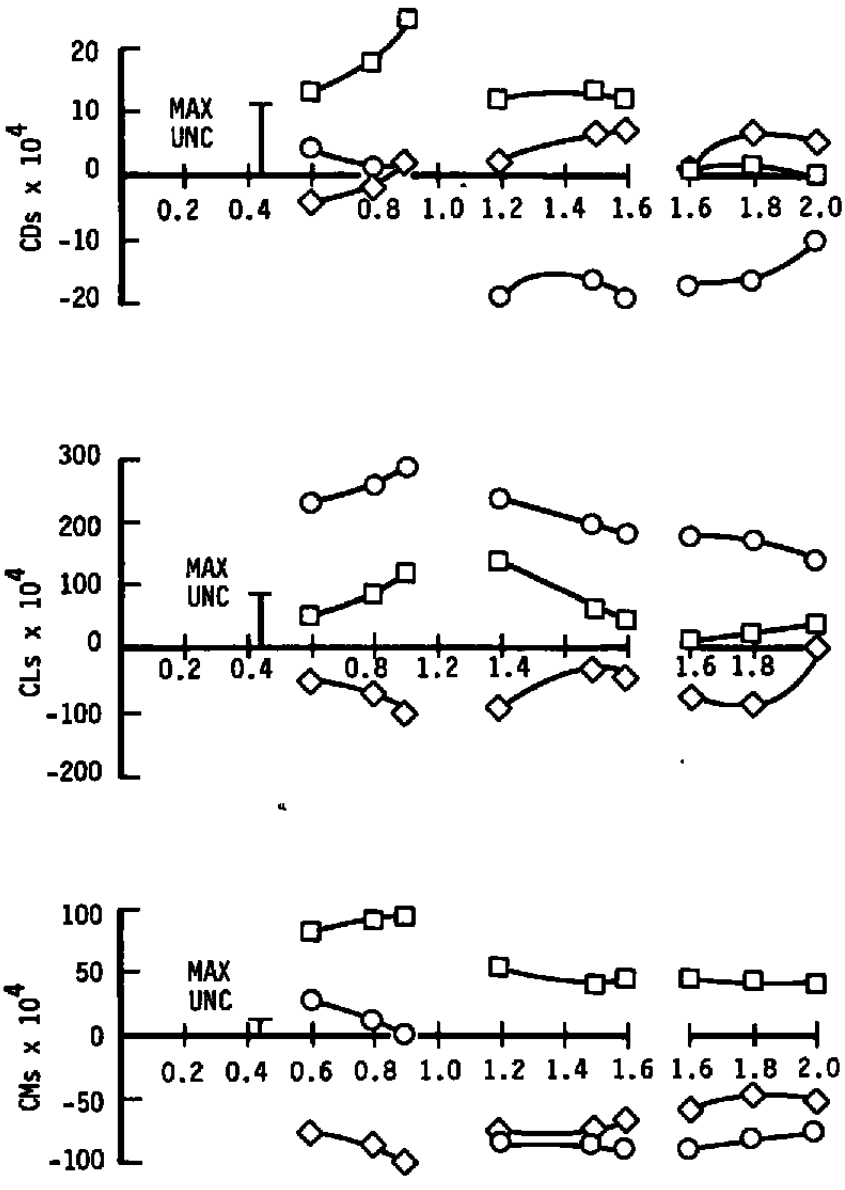


**b. Alpha = 0 deg**
**Figure 8. Continued.**

□ Lower Blade Tail Off

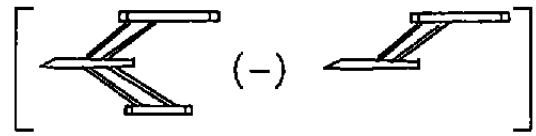

○ Sting Tail Off

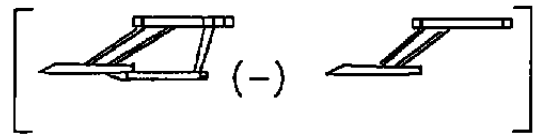

◇ Upper Blade Tail Off

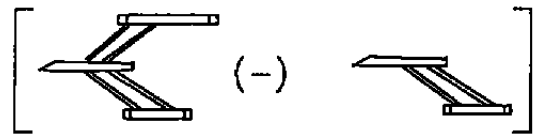

**Legend for Figure 8c**

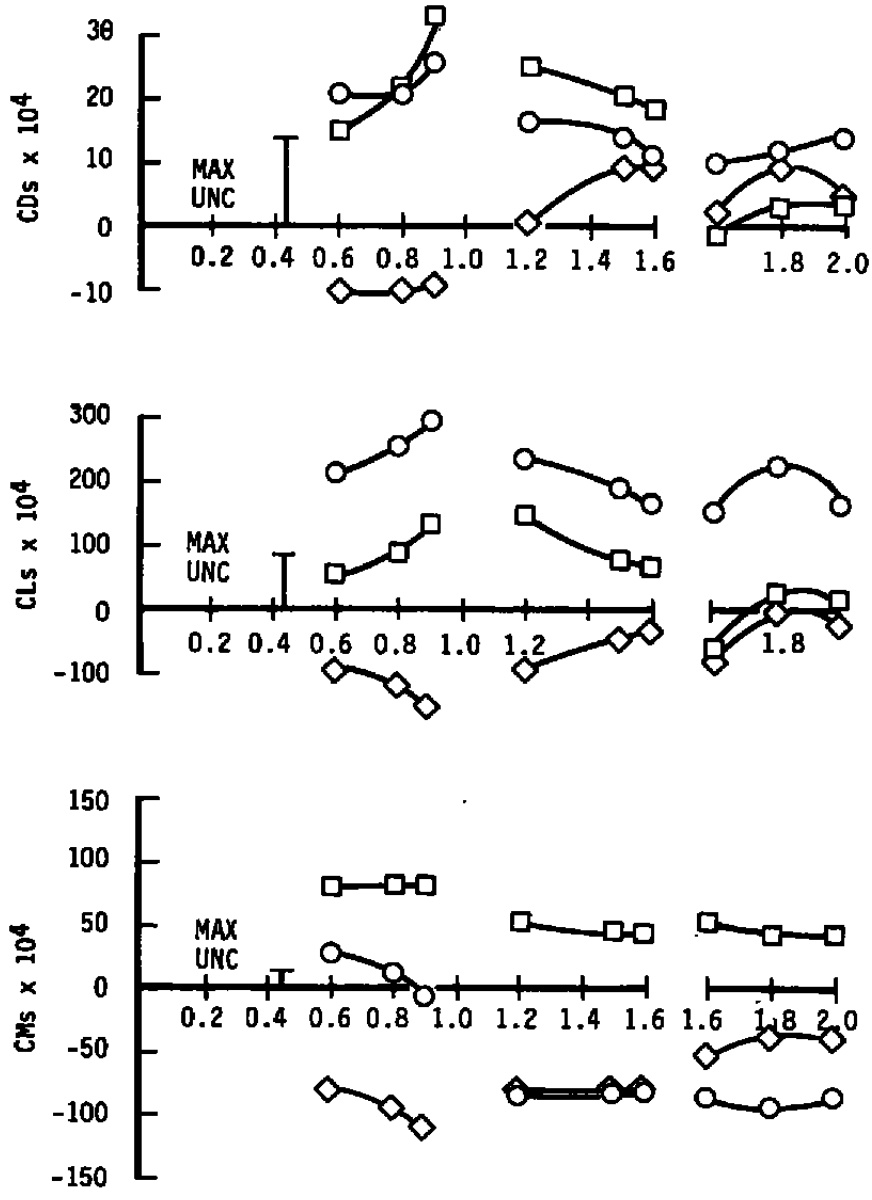


**c. Alpha = 4 deg**

**Figure 8. Continued.**

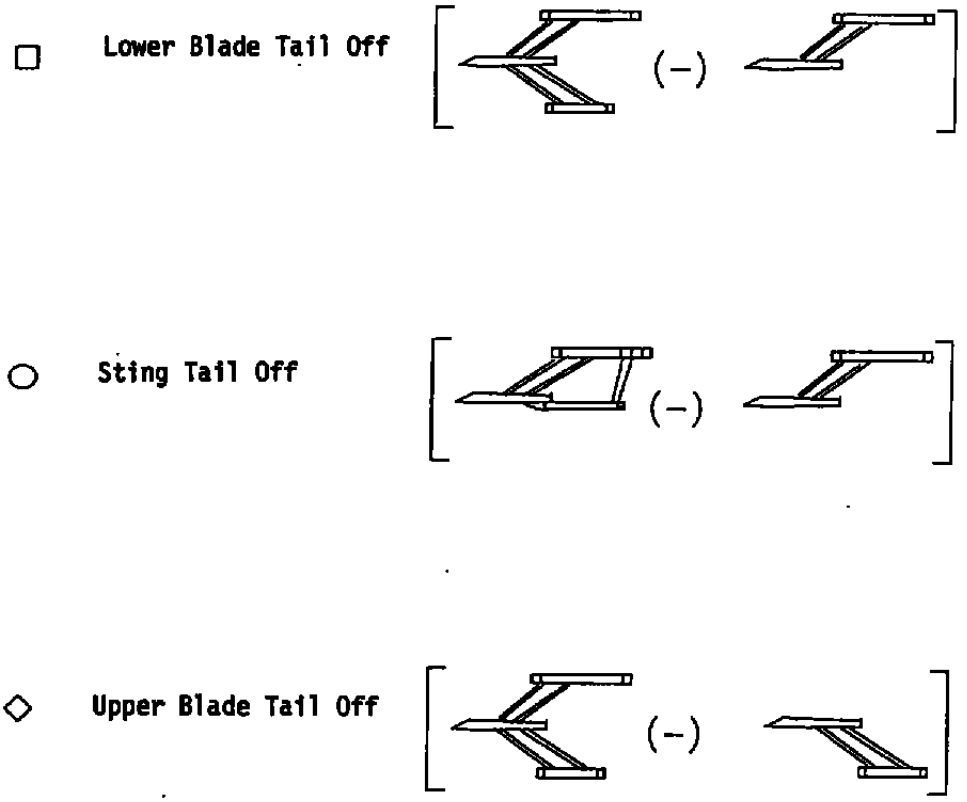


**Legend for Figure 8d**

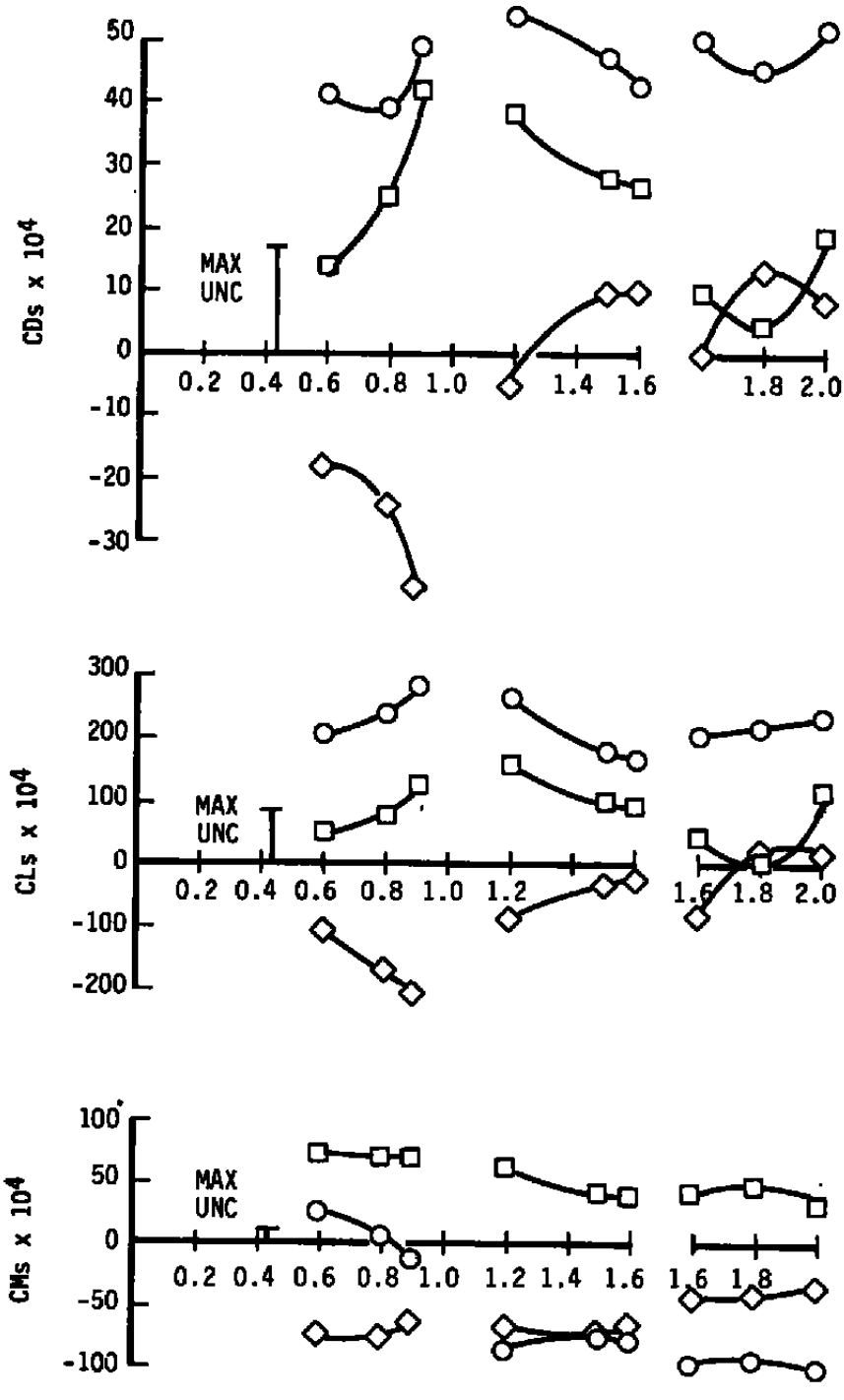


**d. Alpha = 8 deg**
**Figure 8. Concluded.**

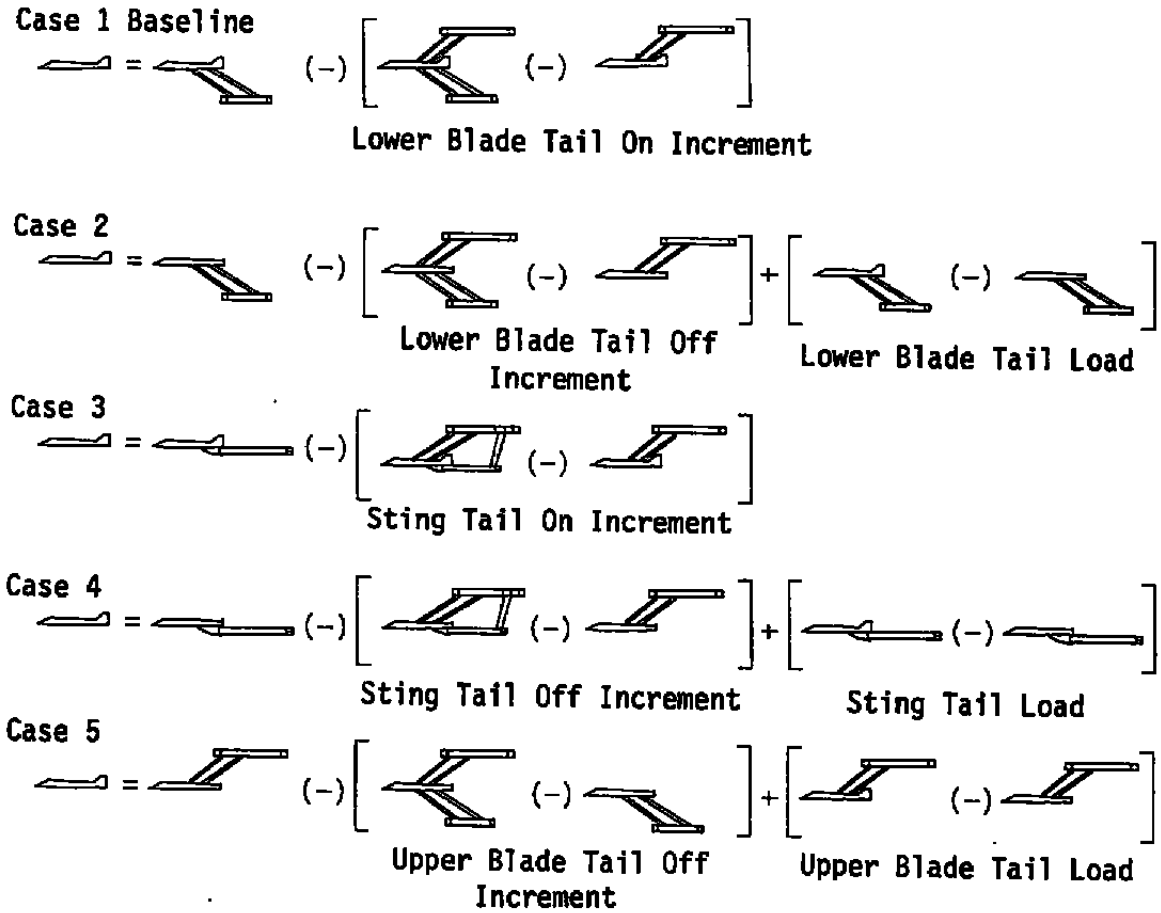


**Figure 9. Support correction methodology.**

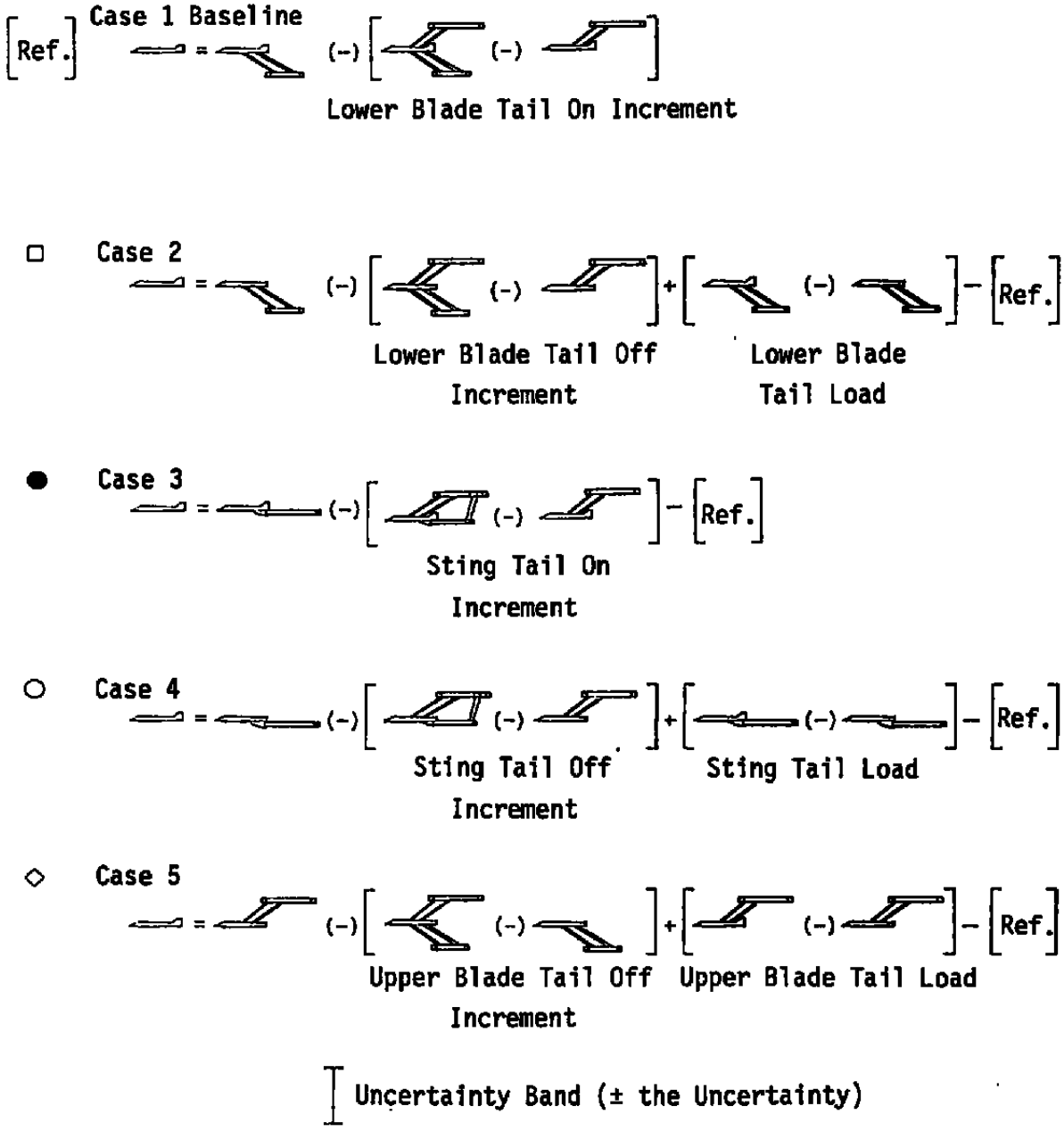


**Legend for Figure 10a**

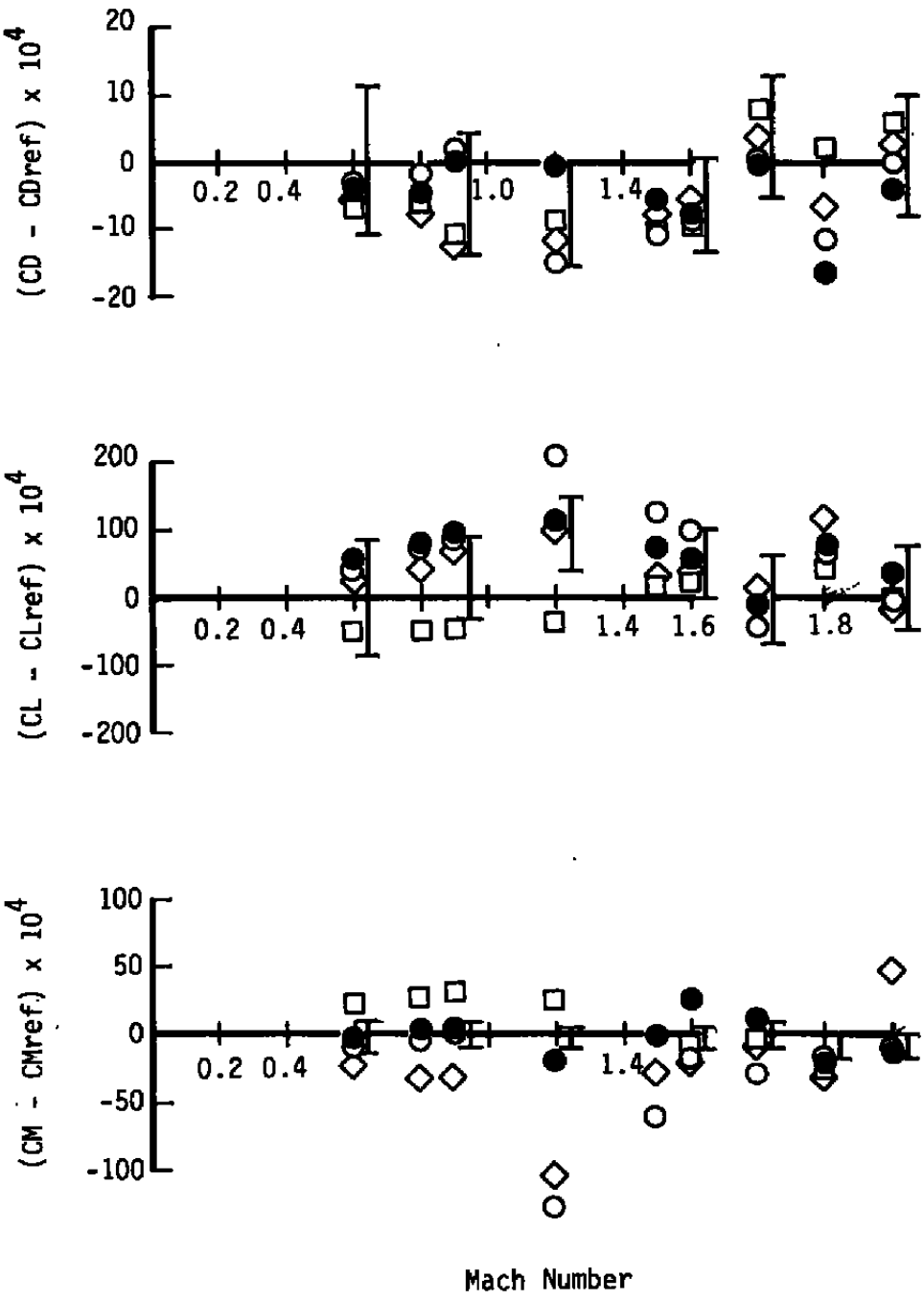


**a. Alpha = −2 deg**

**Figure 10. Comparison of corrections.**

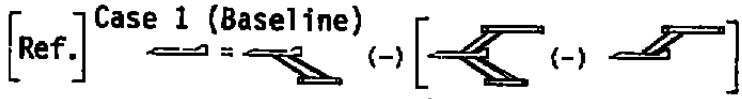


□ Case 2


● Case 3


○ Case 4

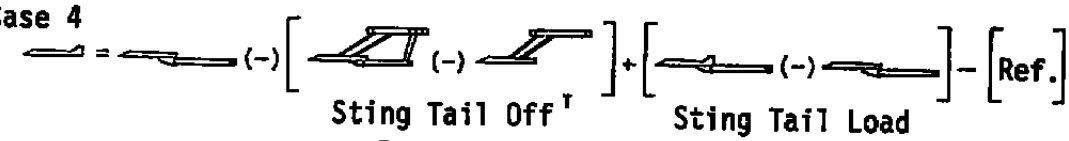


◇ Case 5


Uncertainty Band (± the Uncertainty)

**Legend for Figure 10b**

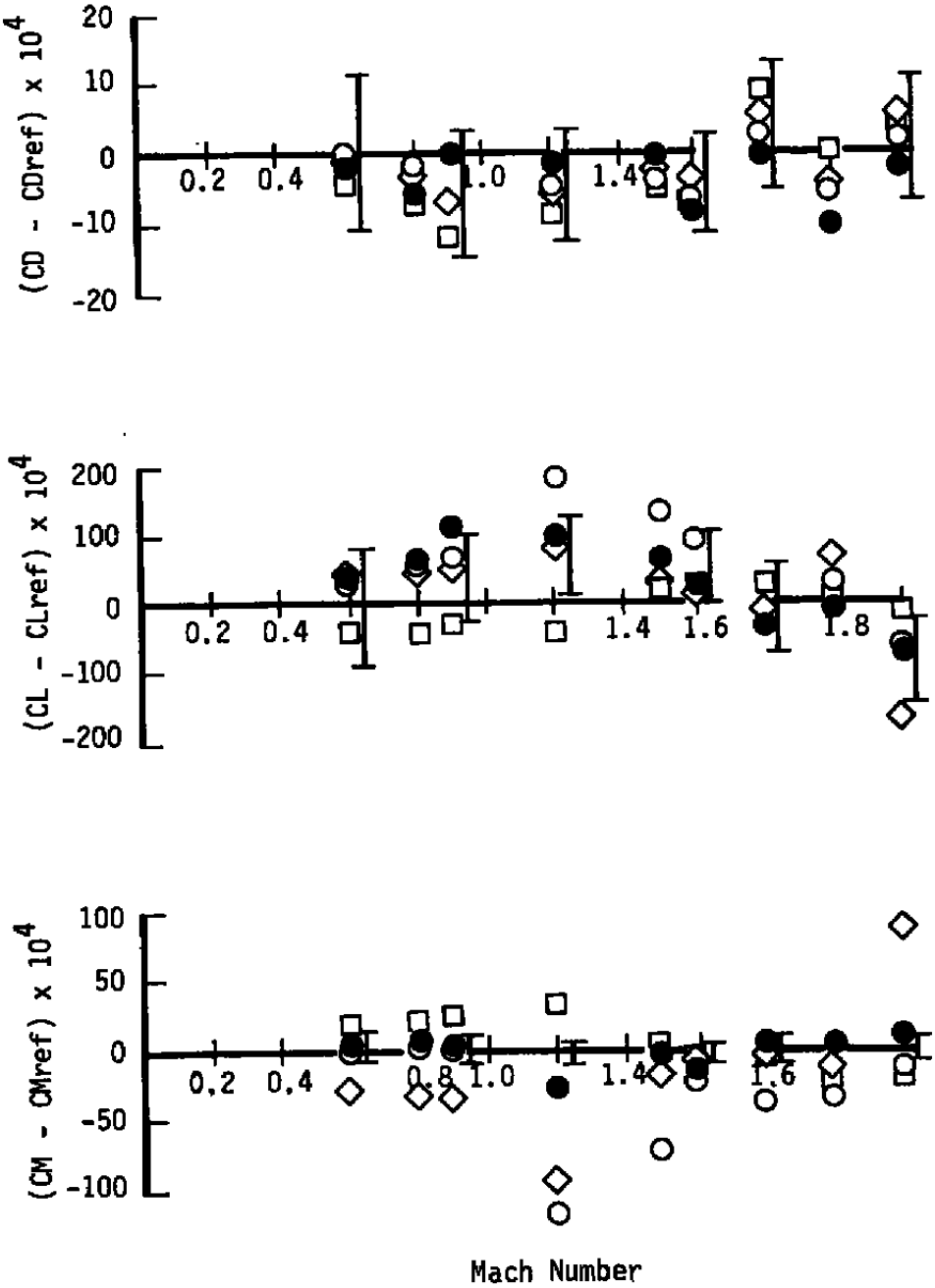


**b. Alpha = 0 deg**

**Figure 10. Continued.**

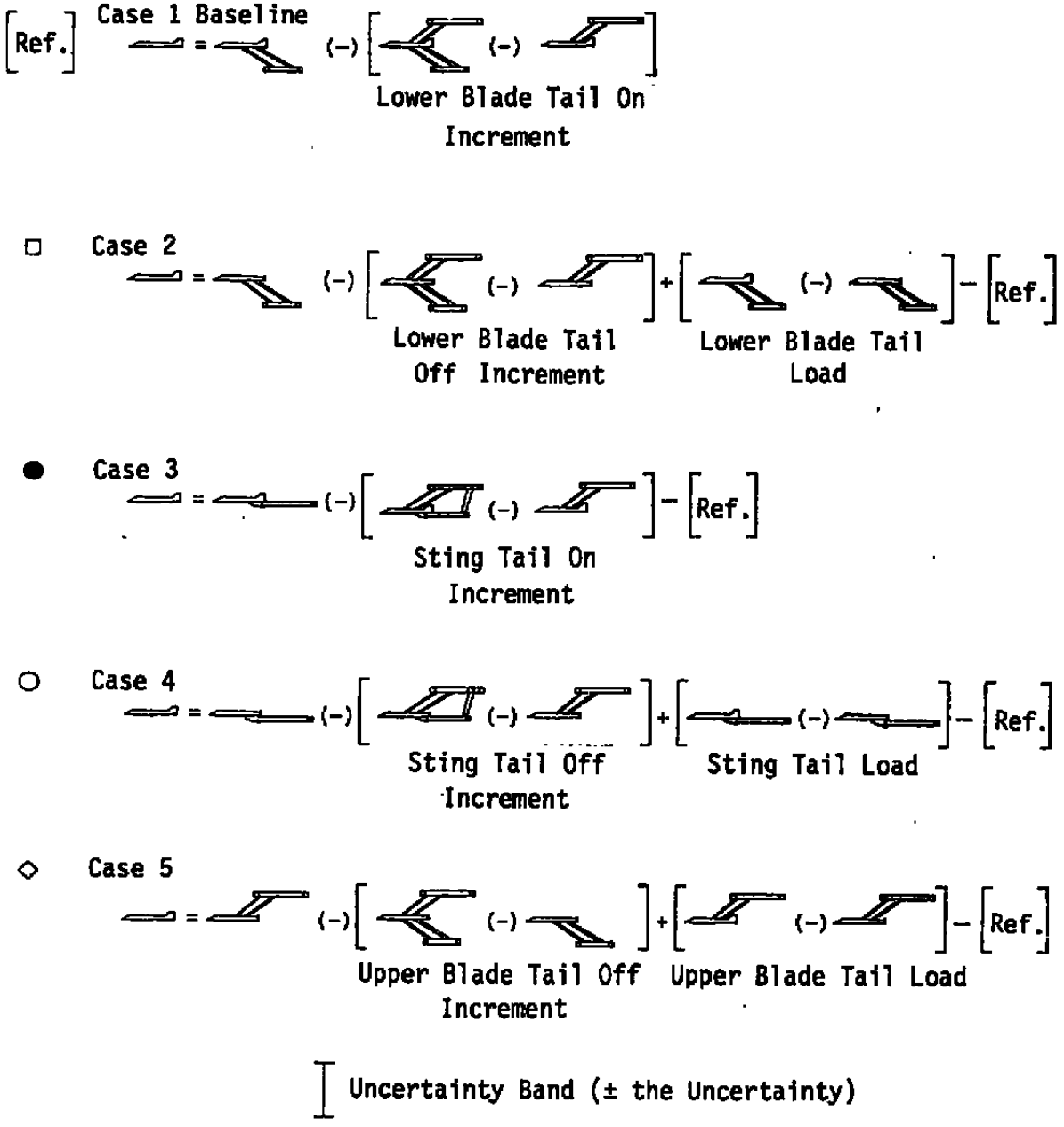


**Legend for Figure 10c**

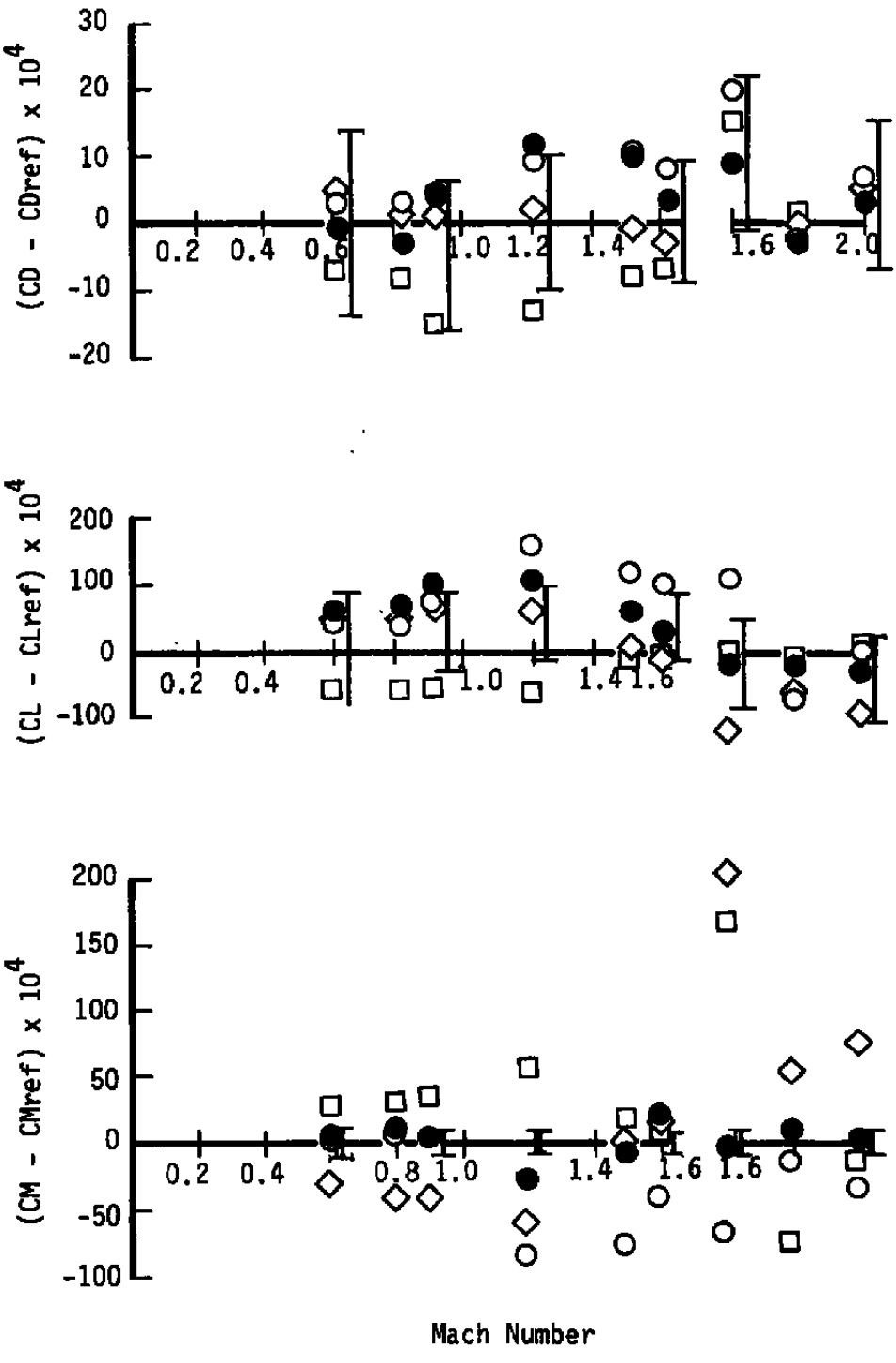


**c. Alpha = 4 deg**
**Figure 10. Continued.**

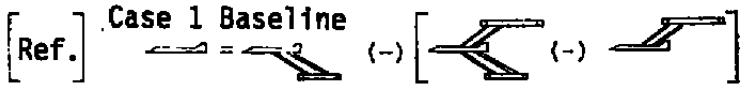


□ Case 2

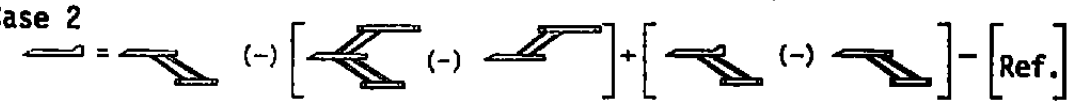


● Case 3


○ Case 4

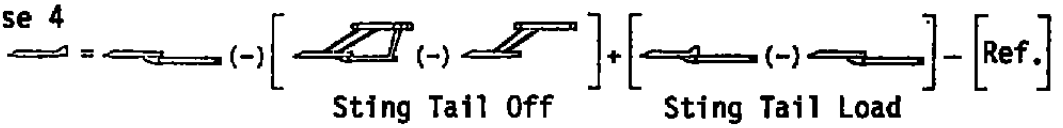


◇ Case 5


I Uncertainty Band (± the Uncertainty)

**Legend for Figure 10d**

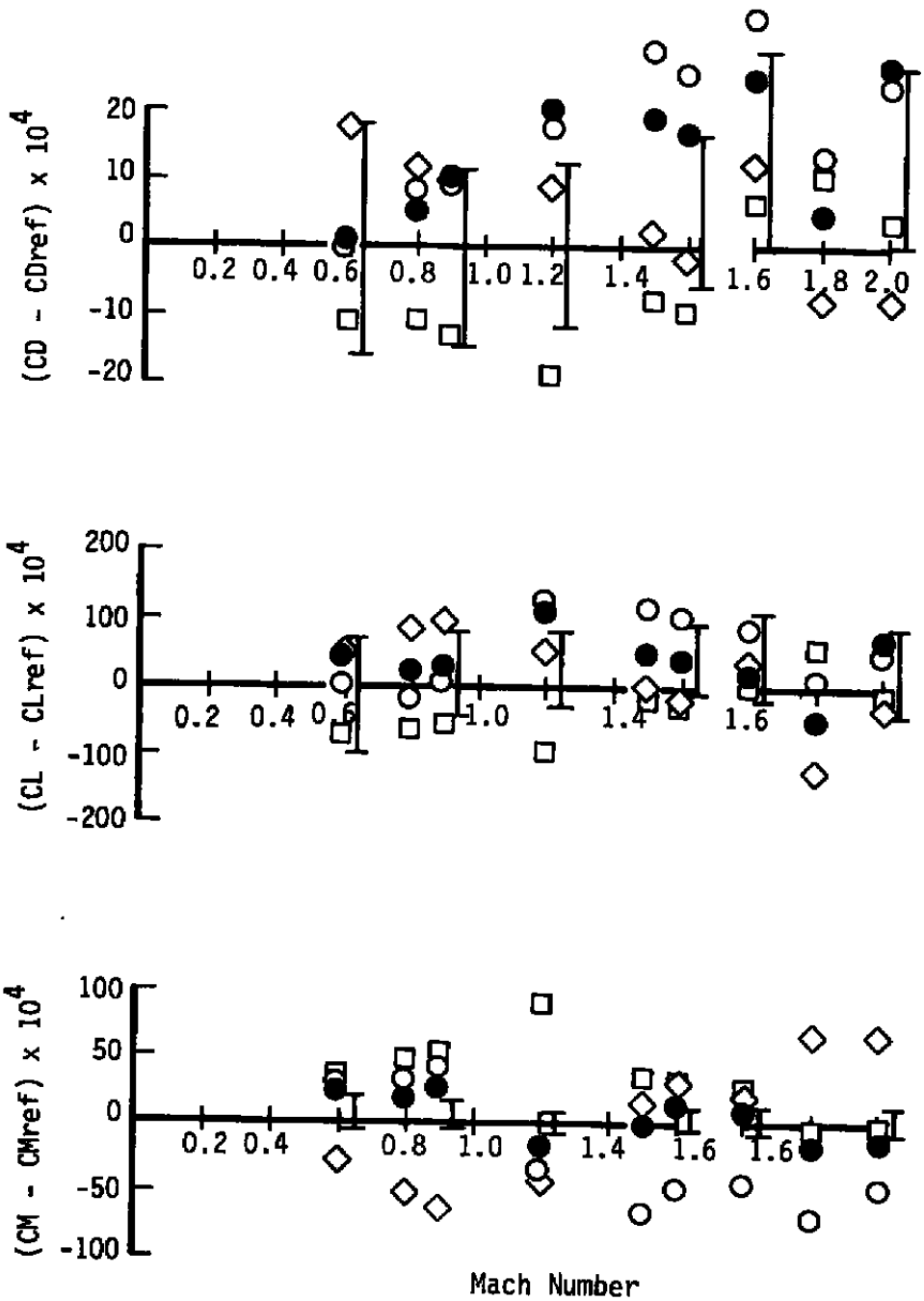


**d. Alpha = 8 deg**

**Figure 10. Concluded.**

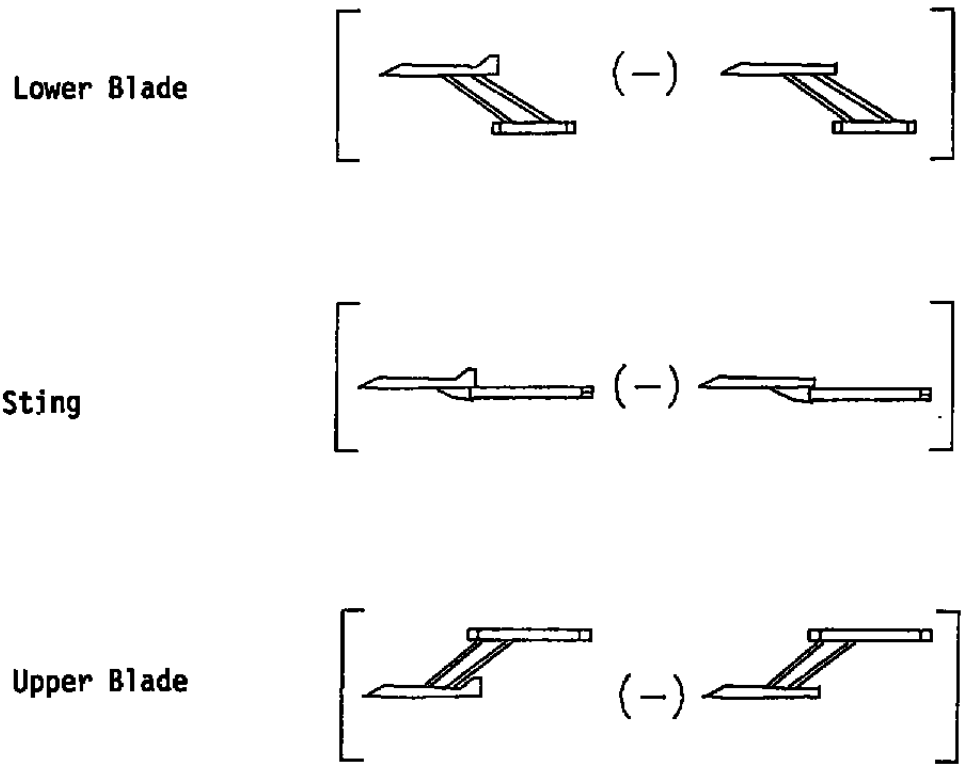


**Figure 11. Tail loads determination.**

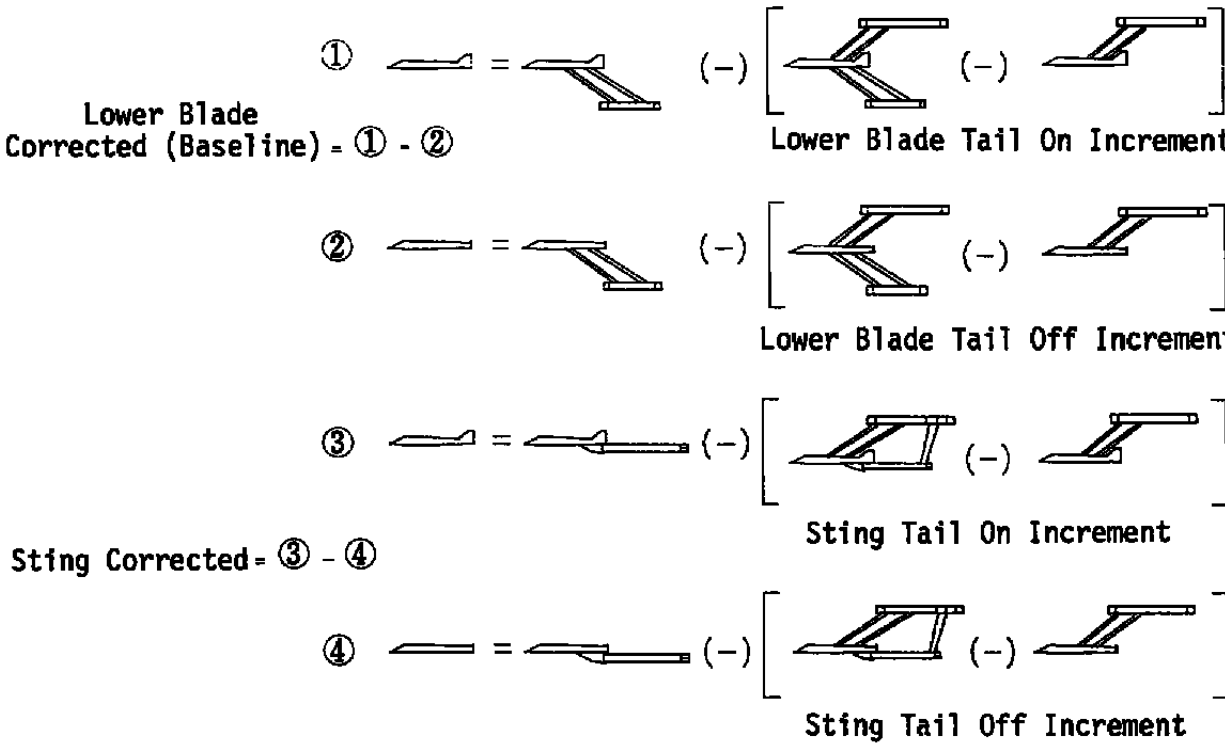


Note: Upper Blade, Corrected is redundant (identical to Lower Blade, Corrected)

**Figure 12. Tail loads correction methodology.**

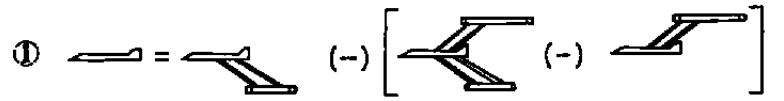


Lower Blade Tail On Increment

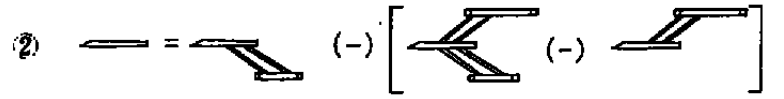


Lower Blade Tail Off Increment

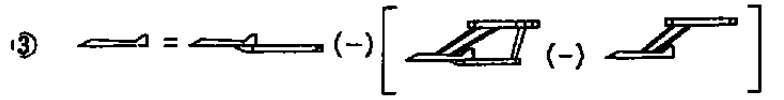


Sting Tail On Increment

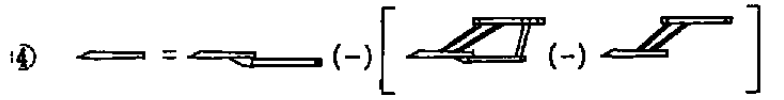


Sting Tail Off Increment

[Ref.] = Lower Blade Corrected = ①-②

● Sting Corrected = ③-④ − [Ref.]

□ Lower Blade 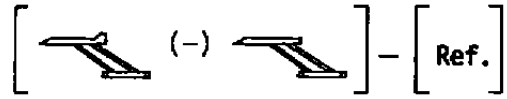


○ Sting 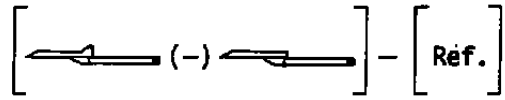


◇ Upper Blade 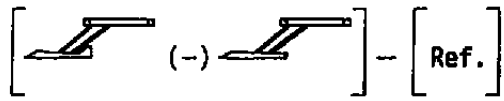


I Uncertainty Band (± the Uncertainty)

**Legend for Figure 13a**

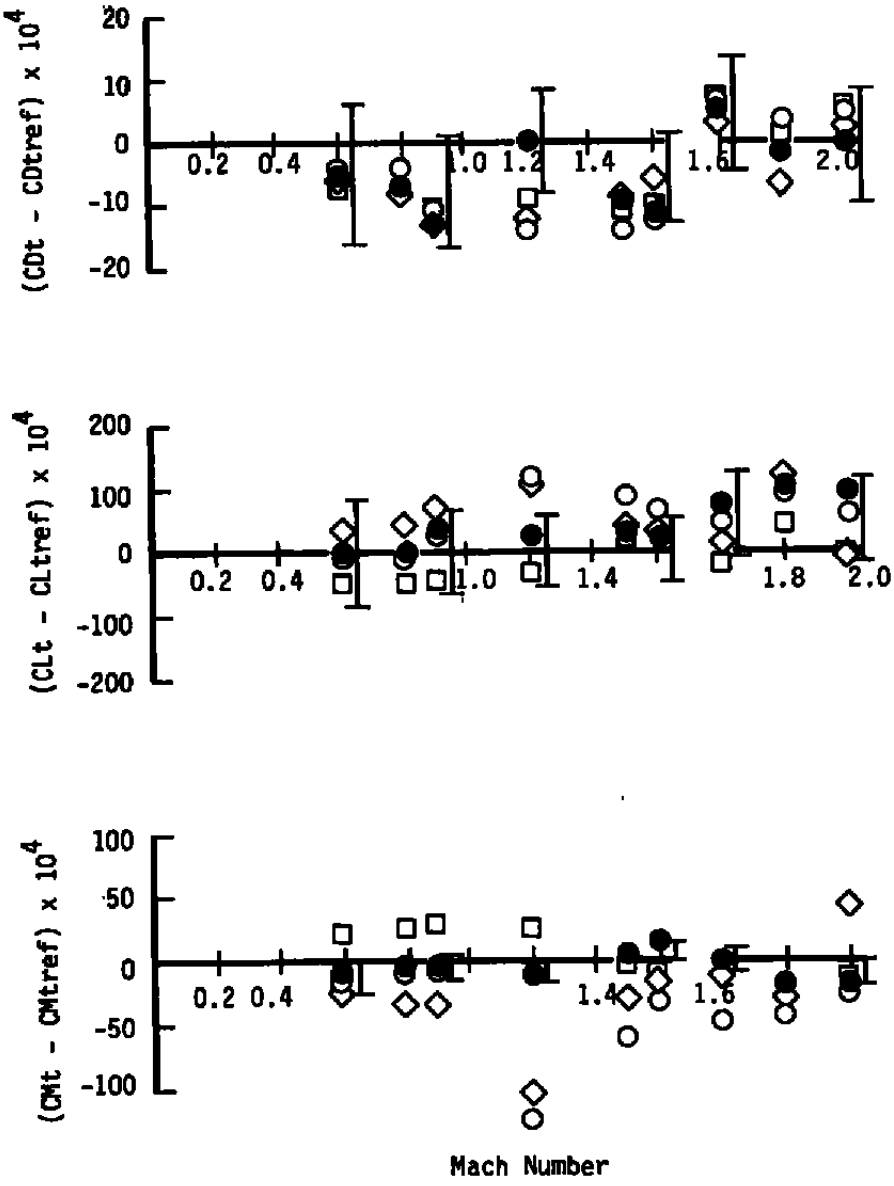


a. Alpha = −2 deg

**Figure 13. Comparison of tail loads and corrections.**

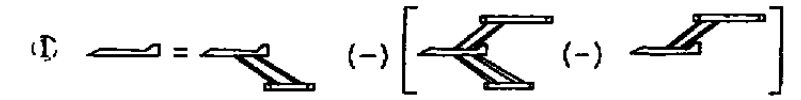


Lower Blade Tail On Increment

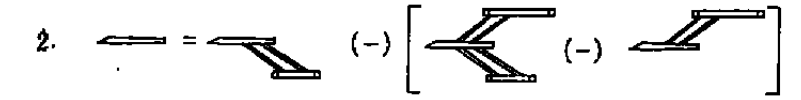


Lower Blade Tail Off Increment

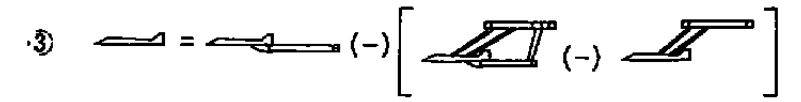


Sting Tail On Increment

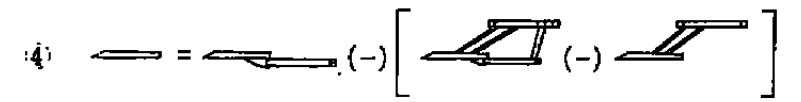


Sting Tail Off Increment

[Ref.] = Lower Blade Corrected = ①-②

● Sting Corrected = ③-④ − [Ref.]

□ Lower Blade [ (-) ] − [Ref.]

○ Sting [ (-) ] − [Ref.]

◇ Upper Blade [ (-) ] − [Ref.]

I Uncertainty Band (± the Uncertainty)

**Legend for Figure 13b**

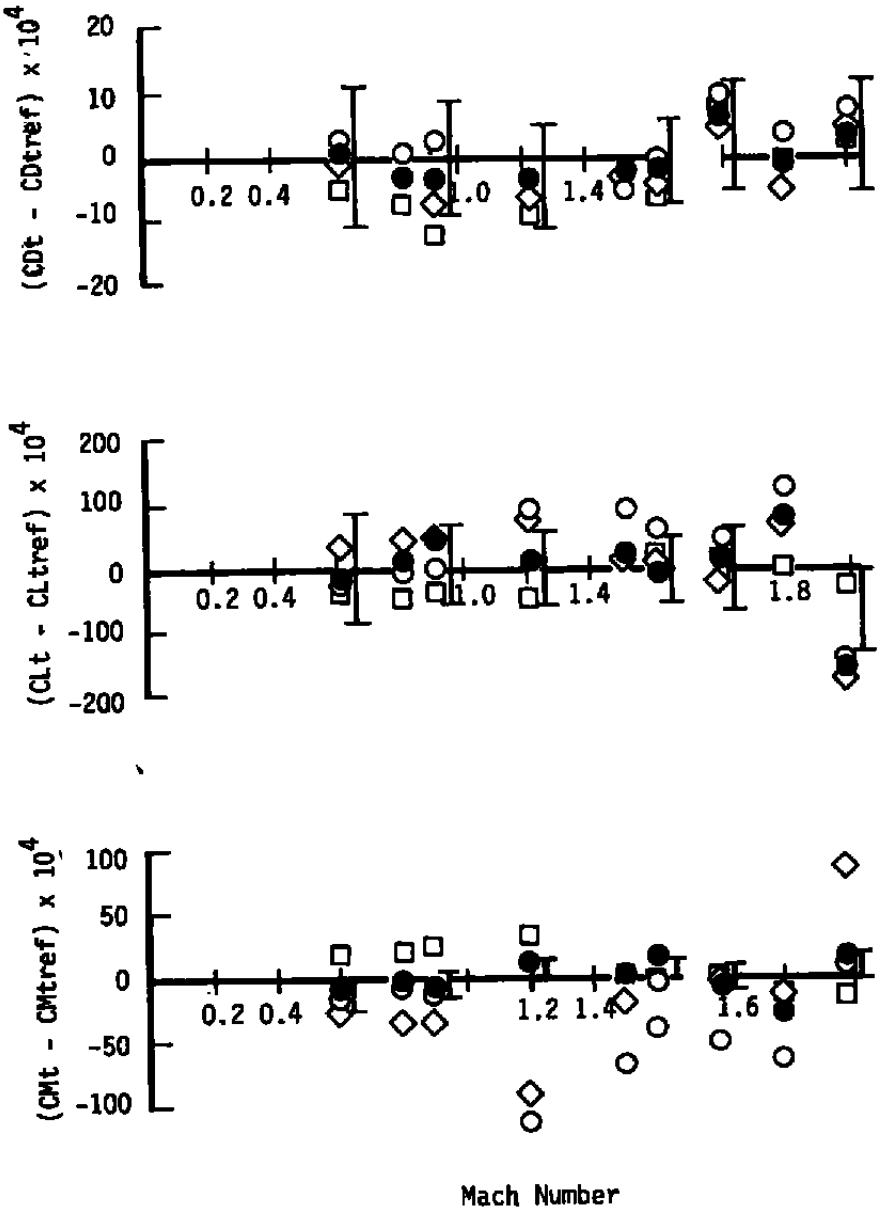


**b. Alpha = 0 deg**
**Figure 13. Continued.**

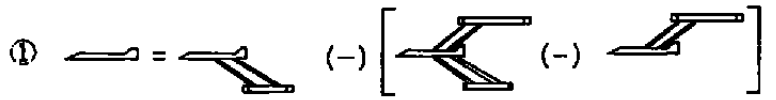


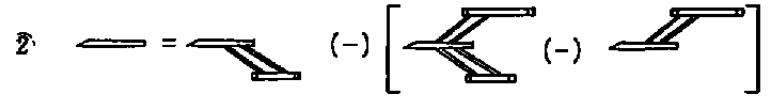


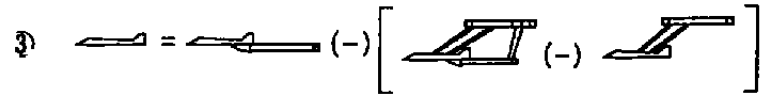


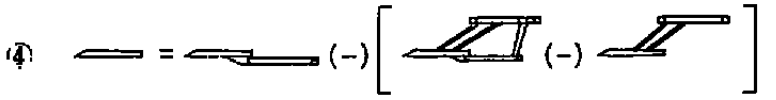


[Ref.] = Lower Blade Corrected = ①-②

● Sting Corrected = ③-④ − [Ref.]

□ Lower Blade [ (-) ] − [Ref.]

○ Sting [ (-) ] − [Ref.]

◇ Upper Blade [ (-) ] − [Ref.]

I Uncertainty Band (± the Uncertainty)

**Legend for Figure 13c**

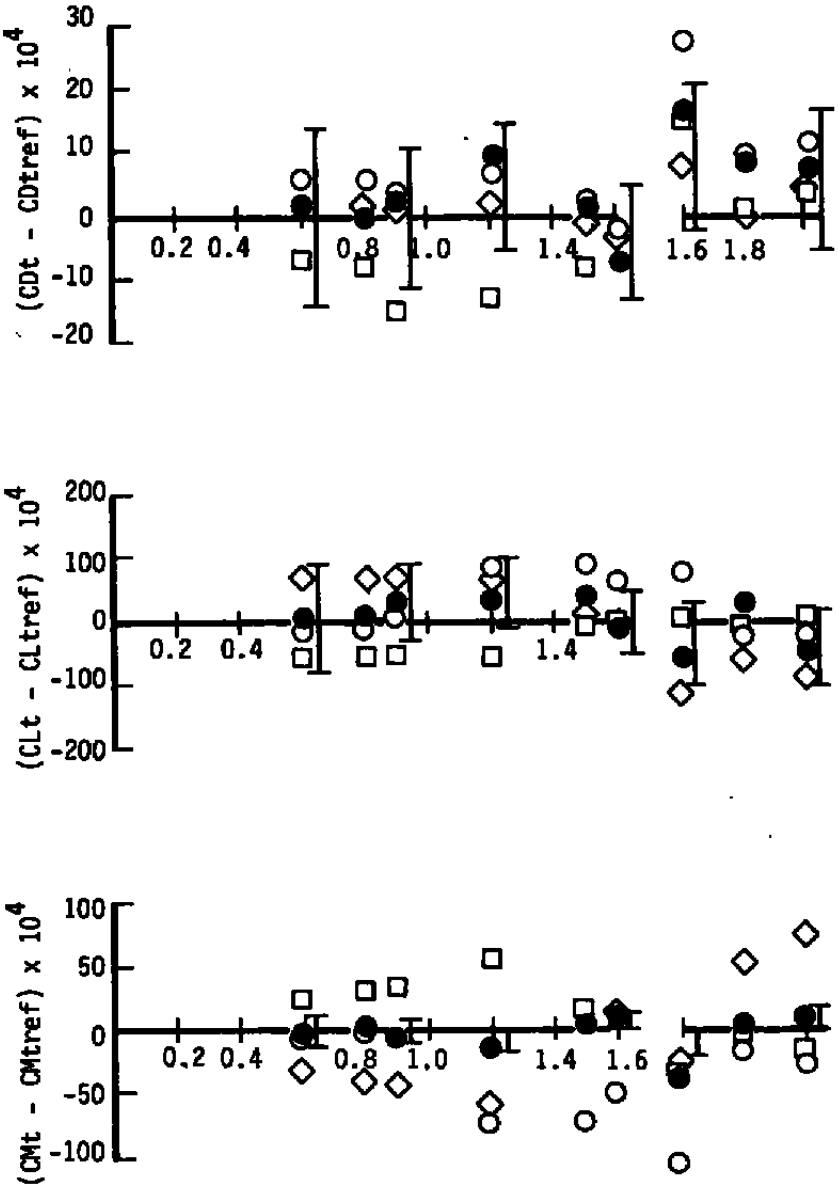


**c. Alpha = 4 deg**

**Figure 13. Continued.**

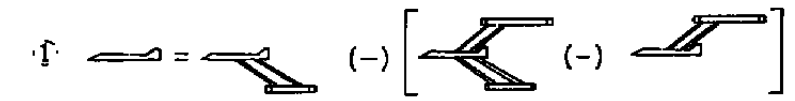


Lower Blade Tail On Increment

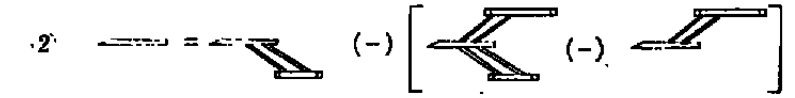


Lower Blade Tail Off Increment

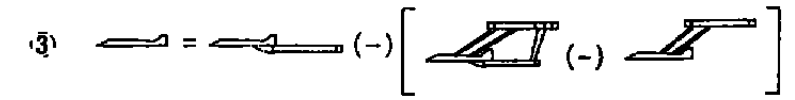


Sting Tail On Increment

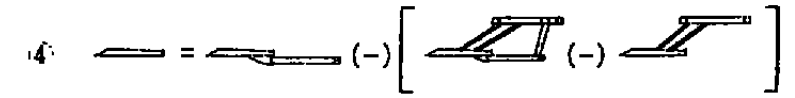


Sting Tail Off Increment

[Ref.] = Lower Blade Corrected = ①-②

● Sting Corrected = ③-④ − [Ref.]

□ Lower Blade [ (-) ] − [Ref.]

○ Sting [ (-) ] − [Ref.]

◇ Upper Blade [ (-) ] − [Ref.]

I Uncertainty Band (± the Uncertainty)

**Legend for Figure 13d**

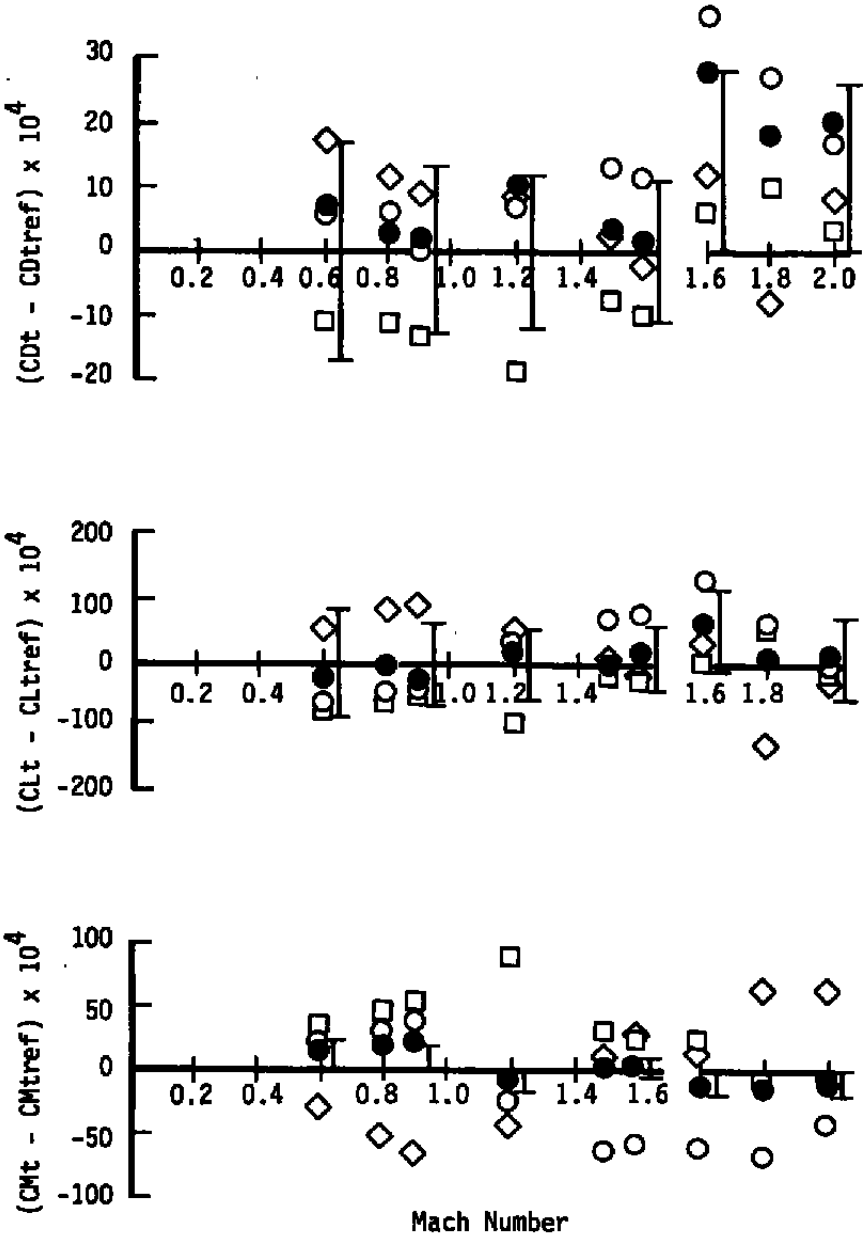


**d. Alpha = 8 deg**

**Figure 13. Concluded.**

**Table 1. Estimated Uncertainties of Basic Test Parameters**

| Tunnel | Configuration | M | Alpha, deg | UAlpha, deg | UCD × $10^4$ | UCL × $10^4$ | UCM × $10^4$ |
|---|---|---|---|---|---|---|---|
| 16T | L BLADE | 0.6 | 0 | 0.052 | 11 | 85 | 12 |
| | L BLADE | 0.6 | 8.0 | | 17 | 84 | 12 |
| | L BLADE | 0.9 | 0 | | 9 | 63 | 9 |
| | | 0.9 | 8.0 | | 13 | 63 | 9 |
| | | 1.2 | 0 | | 8 | 55 | 8 |
| | | 1.2 | 8.0 | | 12 | 55 | 8 |
| | | 1.6 | 0 | | 7 | 51 | 7 |
| 16T | | | 8.0 | | 11 | 51 | 7 |
| 16S | | | 0 | | 9 | 65 | 9 |
| | | 1.6 | 8.0 | | 14 | 65 | |
| | | 2.0 | 0 | | 9 | 66 | |
| 16S | L BLADE | 2.0 | 8.0 | | 13 | 66 | |
| 16T | U BLADE | 0.9 | 0 | | 9 | 63 | |
| 16T | STING | 0.9 | 0 | 0.052 | 9 | 63 | 9 |

**Table 2. Repeatability of Basic Test Parameters**

| M | Alpha, deg | DCDavg $\times 10^4$ | DCDmax $\times 10^4$ | DCLavg $\times 10^4$ | DCLmax $\times 10^4$ | DCMavg $\times 10^4$ | DCMmax $\times 10^4$ | Condition No. |
|---|---|---|---|---|---|---|---|---|
| 0.6 | 0 | 26 | 26 | 3 | 3 | 0 | 0 | 2 |
| 0.6 | 8.0 | 5 | 5 | 12 | 12 | 0 | 0 | 2 |
| 0.9 | 0 | 4 | 9 | 23 | 38 | 2 | 3 | 8 |
| 0.9 | 8.0 | 2 | 4 | 7 | 8 | 2 | 2 | 4 |
| 1.2 | 0 | 1 | 1 | 3 | 4 | 5 | 8 | 6 |
| 1.2 | 8.0 | 1 | 1 | 3 | 3 | 2 | 2 | 2 |
| 1.6 (16T) | 0 | 6 | 6 | 0 | 0 | 0 | 0 | 2 |
| 1.6 (16T) | 8.0 | 7 | 7 | 7 | 7 | 3 | 3 | 2 |
| 1.6 (16S) | 0 | 5 | 11 | 18 | 38 | 10 | 20 | 7 |
| 1.6 (16S) | 8.0 | 12 | 14 | 49 | 74 | 10 | 18 | 5 |
| 2.0 | 0 | 3 | 3 | 21 | 21 | 9 | 9 | 2 |
| 2.0 | 8.0 | 0 | 0 | 16 | 16 | 5 | 5 | 2 |

## NOMENCLATURE

| | |
|---|---|
| Alpha | Model angle of attack, deg |
| b | Model wing span, in. |
| $\bar{c}$ | Model mean aerodynamic chord, in. |
| CD | Drag coefficient for total body |
| CDref | Baseline total body drag coefficient |
| CDs | Drag coefficient due to support system |
| CDt | Drag coefficient for tail |
| CDtref | Baseline tail drag coefficient |
| CL | Lift coefficient for total body |
| CLref | Baseline total body lift coefficient |
| CLs | Lift coefficient due to support system |
| CLt | Lift coefficient for tail |
| CLtref | Baseline tail lift coefficient |
| Condition No. | Number of repeat runs for a given condition |
| CM | Pitching-moment coefficient for total body |
| CMref | Baseline total body pitching-moment coefficient |
| CMs | Pitching-moment coefficient due to support system |
| CMt | Pitching-moment coefficient for tail |
| CMtref | Baseline tail pitching-moment coefficient |

| | |
|---|---|
| DCDavg | Average drag coefficient repeatability |
| DCDmax | Maximum drag coefficient repeatability |
| DCLavg | Average lift coefficient repeatability |
| DCLmax | Maximum lift coefficient repeatability |
| DCMavg | Average pitching-moment coefficient repeatability |
| DCMmax | Maximum pitching-moment coefficient repeatability |
| ESP | Electronically scanned pressures |
| HAAS | High-angle automated sting |
| L BLADE | Lower blade |
| M | Free-stream Mach number |
| MAX UNC | Maximum uncertainty |
| S | Model wind reference area, $ft^2$ |
| UAlpha | Uncertainty of model angle of attack, deg |
| U BLADE | Upper blade |
| UCD | Uncertainty of drag coefficient |
| UCL | Uncertainty of lift coefficient |
| UCM | Uncertainty of pitching-moment coefficient |